

Chiral Emission from Optical Metasurfaces and Metacavities

Jungho Han, Heejoo Jang, Yeonsoo Lim, Seongheon Kim, Jeheon Lee, and Young Chul Jun*

Chiral emission exhibiting a large degree of circular polarization (DCP) is important in diverse applications ranging from displays and optical storage to optical communication, bioimaging, and medical diagnostics. Although chiral luminescent materials can generate chiral emissions directly, they frequently suffer from either low DCP or low quantum efficiencies. Achieving high DCP and quantum efficiencies simultaneously remains extremely challenging. This review introduces an alternative approach to chiral emission. Chiral emission with large DCP can be readily achieved by combining conventional achiral emitters with chiral metasurfaces. Particularly, this article focuses on recent experimental and theoretical studies on perovskite metasurfaces and metacavities that employ achiral perovskite materials. First, chiral photoluminescence from extrinsic and intrinsic perovskite metasurfaces is explained together with theoretical discussions on metasurface design based on reciprocity and critical coupling. Chiral photoluminescence from other achiral materials is also explained. Subsequently, chiral electroluminescence from perovskite metacavities and other achiral materials is discussed. Finally, it is concluded with future perspectives. This review provides physical insights into how ideal chiral emission can be realized by optimizing the design of metasurfaces and metacavities. Compact chiral light sources with both near-unity DCP and strong emission intensities can have far-reaching consequences in a wide range of future applications.

be superimposed onto their mirror images. Such chiral objects can be obtained by breaking the mirror symmetries of the objects and they can respond differently to incident left circularly polarized (LCP) and right circularly polarized (RCP) light. Numerous natural materials including amino acids, deoxyribonucleic acids (DNA), proteins, and sugars exhibit chiral optical (chiroptical) responses such as circular dichroism and optical activity. However, the chiral responses in natural materials are typically weak. To address this challenge, both intrinsic and extrinsic chirality in plasmonic and dielectric resonant nanostructures have been widely studied to substantially enhance the chiral responses.^[6–13] Intrinsic chirality originates from the geometric properties of mirror-symmetry-broken nanostructures; meanwhile, extrinsic chirality also considers light illumination conditions (Figure 1a,b).^[14,15] Therefore, extrinsic chirality can emerge even in optical nanostructures with mirror symmetry. Due to the Lorentz reciprocity, the chiral effects in the linear optical regime can

1. Introduction


Chirality is widespread in nature.^[1–5] It can be observed at significantly different scales ranging from subatomic particles and biomolecules to spiral galaxies. In general, chiral objects cannot

be achieved intrinsically by breaking structural mirror symmetries or extrinsically by misaligning the direction of the excitation beam with the symmetry axes.^[16] Three-dimensional (3D) nanostructures, such as helices, twisted multilayers, and gyroid structures, can exhibit intrinsic chirality.^[8,17–22] However, because of the fabrication challenges of such 3D nanostructures, two-dimensional (2D) planar chiral structures (e.g., gammadions and z-shaped structures) have been extensively studied by the nano-optics community.^[17–19,23–26] Planar intrinsic chirality in such 2D chiral structures can exhibit strong chiroptical responses at normal incidence without mirror symmetry breaking in the normal (out-of-plane) direction. However, in contrast to 3D intrinsic chirality, such planar chiral structures exhibit opposite chiral responses when light is illuminated from the bottom because of the reversed rotational direction of the chiral structure. Planar chiral structures with anisotropic geometries can also exhibit circular polarization conversion at normal incidence.

Metasurfaces have been employed as a general platform for chiroptical studies with unprecedented design flexibility compared with natural materials.^[27–31] Highly enhanced chiral

J. Han, Y. Lim, S. Kim, J. Lee, Y. C. Jun
Department of Materials Science and Engineering
Ulsan National Institute of Science and Technology (UNIST)
Ulsan 44919, Republic of Korea
E-mail: ycjun@unist.ac.kr

H. Jang, Y. C. Jun
Graduate School of Semiconductor Materials and Devices Engineering
UNIST
Ulsan 44919, Republic of Korea

 The ORCID identification number(s) for the author(s) of this article can be found under <https://doi.org/10.1002/adpr.202400060>.

© 2024 The Author(s). Advanced Photonics Research published by Wiley-VCH GmbH. This is an open access article under the terms of the Creative Commons Attribution License, which permits use, distribution and reproduction in any medium, provided the original work is properly cited.

DOI: 10.1002/adpr.202400060

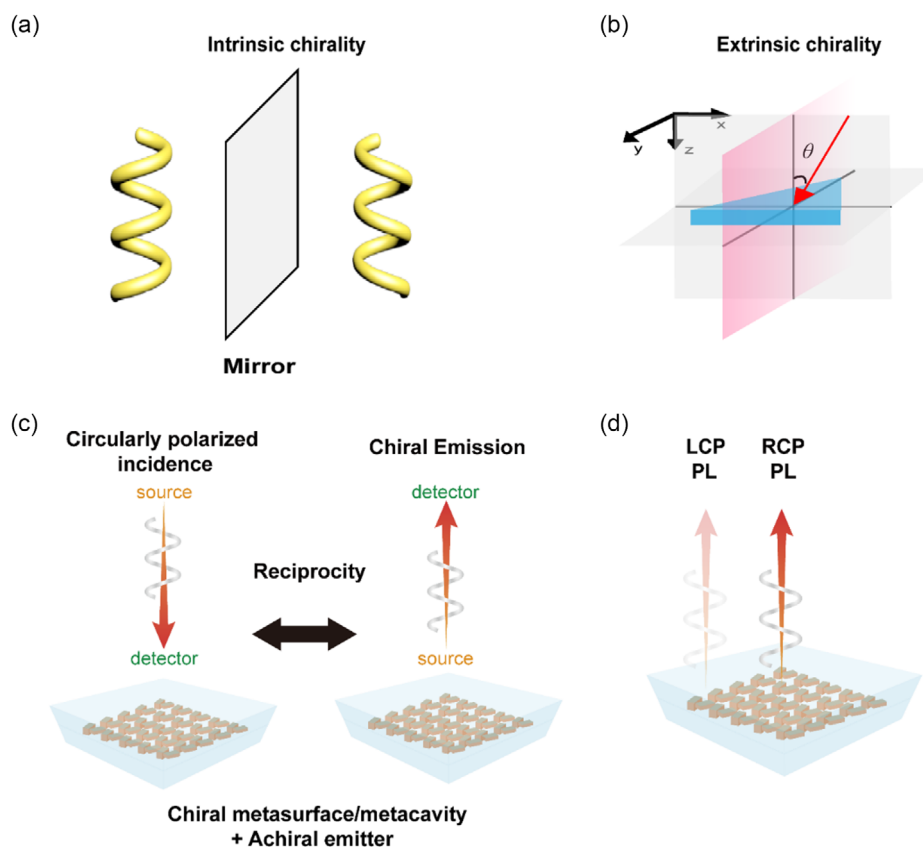


Figure 1. Intrinsic and extrinsic chirality. Schematic for a) intrinsic chirality and b) extrinsic chirality. Intrinsic chirality originates from the geometric properties of the mirror-symmetry-broken nanostructures, whereas extrinsic chirality considers the light illumination condition as well. Although the triangular pattern in (b) has a mirror symmetry plane (e.g., yz -plane), it can have chiral responses at an oblique incident angle θ . c) Schematic for the reciprocity calculation. Chiral emission can be calculated by integrating the field enhancement in a light-emitting medium under circularly polarized light incidence. d) In ideal chiral light sources, light emission for one helicity (e.g., right circularly polarized or RCP emission) is strongly enhanced while the other helicity (e.g., left circularly polarized or LCP emission) is suppressed. Reproduced with permission.^[60] Copyright 2023, Wiley-VCH.

light–matter interactions in metasurfaces are essential in important applications including enantiomer selection, chiral molecular sensing, chiral quantum optics, and quantum materials engineering.^[32–39] Circular dichroism (CD) indicates a difference in the outcomes of light–matter interaction. It is a commonly used parameter to characterize the chiral responses of metasurfaces in reflection, transmission, and absorption. For example, CD for transmission is commonly defined as $CD_T = (T_R - T_L) / (T_R + T_L)$, where $T_{R(L)}$ is the transmittance under RCP (LCP) illumination.

Particularly, chiral light emitters exhibiting a large degree of circular polarization (DCP) are highly desirable in technologies ranging from displays and optical storage to optical communication, bioimaging, and medical diagnostics.^[40–45] The DCP is a key parameter characterizing emission chirality. DCP ρ_c is defined as the ratio of RCP to LCP emission intensities: $\rho_c = (I_{RCP} - I_{LCP}) / (I_{RCP} + I_{LCP})$. The DCP value ranges from -1 to 1 ; its magnitude lies between 0 and 1 , and its sign can be either positive or negative (corresponding to the RCP or LCP emission). It is also related to the normalized Stokes parameter: $\rho_c = S_3 / S_0$. Note that luminescence dissymmetry factor g_{lum} is another common parameter to characterize chiral emission

(usually used for chiral molecules), which is related to DCP as follows: $g_{lum} = 2(I_{RCP} - I_{LCP}) / (I_{RCP} + I_{LCP}) = 2\rho_c$. In general, chiral light sources can be constructed using a linear polarizer and quarter-wave plate. However, these bulky optical elements are undesirable for integrated device platforms. The direct generation of chiral emission from luminescent materials would enable the development of various compact devices. Chiral luminescent materials such as chiral perovskites, conjugated polymers, and metal complexes can be used to generate chiral emission.^[46–56] However, these chiral materials often suffer from either low DCP or low internal/external quantum efficiencies. Achieving high DCP and quantum efficiencies simultaneously at room temperature remains extremely challenging. For recent progresses in chiral luminescent materials, refer to recent reviews on chiral organic materials^[46–48,57] and chiral perovskites.^[49,50]

Here, we introduce an alternative approach to chiral emission. Chiral emission with large DCP can be achieved by combining conventional *achiral* emitters (such as dye molecules, semiconductor quantum wells or dots, and perovskite materials) with chiral metasurfaces. Achiral emitters with high internal quantum efficiencies can be employed for chiral emission using intrinsic

or extrinsic chiral nanostructures. In this article, we review the recent progresses in chiral emission from optical metasurfaces and metacavities. Particularly, we mainly discuss recent experimental and theoretical studies on perovskite metasurfaces and metacavities conducted within our own research group.^[58–62] Lead halide perovskites, including hybrid organic–inorganic and all-inorganic perovskites, have a significant potential for use in light-emitting devices owing to their ability to exhibit high photoluminescence (PL) quantum yields, high color purity (or narrow emission linewidth), and high charge-carrier mobility.^[63–72] The widely tunable bandgap energy makes perovskite materials ideal light sources in the visible spectral range. Chiral perovskite materials can be created by incorporating chiral organic ligands on the surface of perovskite crystals or by intercalating chiral organic cations into the perovskite lattice; however, they typically exhibit a low DCP. Although chiral perovskites can enable the direct optical control of spin polarization, DCP is typically limited to a few percent at room temperature because of the fast spin relaxation (on the order of picoseconds) relative to the long radiative recombination time (on the order of nanoseconds).^[73,74] Therefore, it is highly desirable to develop alternative strategies to achieve high levels of chiral emission using widely available achiral emitters.

In this review, we introduce chiral PL from extrinsic and intrinsic metasurfaces using achiral perovskite materials. We also review the chiral PL from other achiral emitters. Then, we discuss chiral electroluminescence (EL) from perovskite metacavities and other achiral emitters. In the case of the perovskite metasurface, the metasurface itself can be defined by light-emitting perovskite materials. Note that the refractive index of the perovskite material is higher than that of surrounding materials (PMMA and quartz). Therefore, the perovskite metasurface itself emits light with high levels of circular polarization. For other achiral emitters (dye molecules, quantum dots, etc.), emitters are usually combined with dielectric metasurfaces made of other materials (such as TiO₂ and Si). Finally, we conclude this review with future perspectives including discussions of chiral polariton states in the strong-coupling regime.

This review provides physical insights into the realization of optimal chiral emission by appropriately designing chiral metasurfaces and metacavities. Here, we explain the generation of chiral emission from achiral emitters using the Lorentz reciprocity principle. The light emission problem is converted into the field enhancement calculation under light incidence using the reciprocity principle (Figure 1c). Chiral field enhancement in optical metasurfaces can be properly engineered to obtain optimal chiral emission. The maximized field enhancement for one helicity of circular polarization can be achieved via critical coupling while the field enhancement for the other helicity is strongly suppressed. This chiral field enhancement leads to high levels of chiral emission via reciprocity (Figure 1d). Chiral emission with both near-unity DCP and strong emission intensities is important for the development of ideal chiral light sources.

Before discussing the details of chiral emission, we clarify our definition of circular polarization. The definition follows that in Hecht's book,^[75] the electric field vector rotates clockwise in time for RCP light when looking at an incoming wave. The rotational direction is reversed when we look in the other direction (i.e., the outgoing wave). Circular polarization measurements frequently

involve tricky technical issues such as polarization distortion and artifacts. For more details, refer to recent articles that discuss such technical issues.^[61,76]

2. Chiral Photoluminescence

2.1. Chiral Photoluminescence from Perovskite Metasurfaces Via Extrinsic Chirality

Perovskite metasurfaces introduce nanopatterning in perovskite thin films to induce either localized optical resonances or delocalized (extended) optical modes.^[77–81] Figure 2 explains how a pair of LCP and RCP emissions can be generated from an achiral perovskite film with symmetry-broken patterns on a substrate (Figure 2a).^[58] Figure 2b shows the detailed fabrication procedure. An array of triangular silver nanostructures with relatively large feature sizes (the side length of the triangular pattern: 350 nm) was patterned onto a quartz substrate (silver thickness: 40 nm). The silver patterns were first covered by a 10 nm Al₂O₃ layer. Subsequently, a 210 nm thick perovskite (MAPbI₃) film was spin-coated on top of the silver pattern and annealed for crystallization. Finally, a 10 nm protective layer of poly(methyl methacrylate) (PMMA) was spin-coated on top of the perovskite film. Figure 2c displays the schematic for the side view of the sample, while Figure 2d shows the scanning electron microscopy (SEM) image of the symmetry-broken (triangular) silver patterns (top view).

The angle-resolved reflectance and PL spectra were measured using a custom-built Fourier-plane setup. For Fourier-plane measurements, the back focal plane of the microscope objective was imaged instead of the sample surface.^[82,83] The angle-resolved spectrum could be obtained either by scanning a pinhole over the Fourier plane or using a monochromator slit as the line aperture in the Fourier plane (i.e., single-shot measurement). A linearly polarized diode laser was used as the excitation light source for the PL measurements. The circular polarization of the perovskite emission was measured using a linear polarizer and quarter-wave plate.

The reflection spectrum clearly exhibits Fano resonance features^[84–90] with a highly asymmetric resonance peak because of the interference between the broad background Fabry–Perot resonance of the perovskite slab and the narrow-guided mode resonance resulting from the periodic patterns. Because of the symmetry-broken triangular silver patterns on the substrate, a strong chiral response was induced via extrinsic chirality. Figure 2e,f display the measured differential reflectance ($\Delta R = R_{RCP} - R_{LCP}$) and PL spectra as a function of wavelength λ_0 and in-plane wavevector k_x/k_0 . The in-plane wavevector is defined as $k_x/k_0 = \sin \theta$, where $k_0 = 2\pi/\lambda_0$ (λ_0 is the wavelength of light in freespace) and θ is the emission angle along the x -axis. $\theta = 0^\circ$ (or $k_x = 0$) indicates the normal direction. The difference in the spectral position between the reflectance and PL spectra can be attributed to the manifestation of chiral Fano resonances. In particular, chiral emission can be strongly enhanced in the narrow-mode position of chiral Fano resonances. High levels of chiral perovskite emission (DCP ≈ 0.524) were obtained at room temperature at relatively small emission angles below 10° (Figure 2e). This design does not involve direct patterning of the perovskite layer. Therefore, the exceptional optoelectronic properties of the perovskites can be preserved.

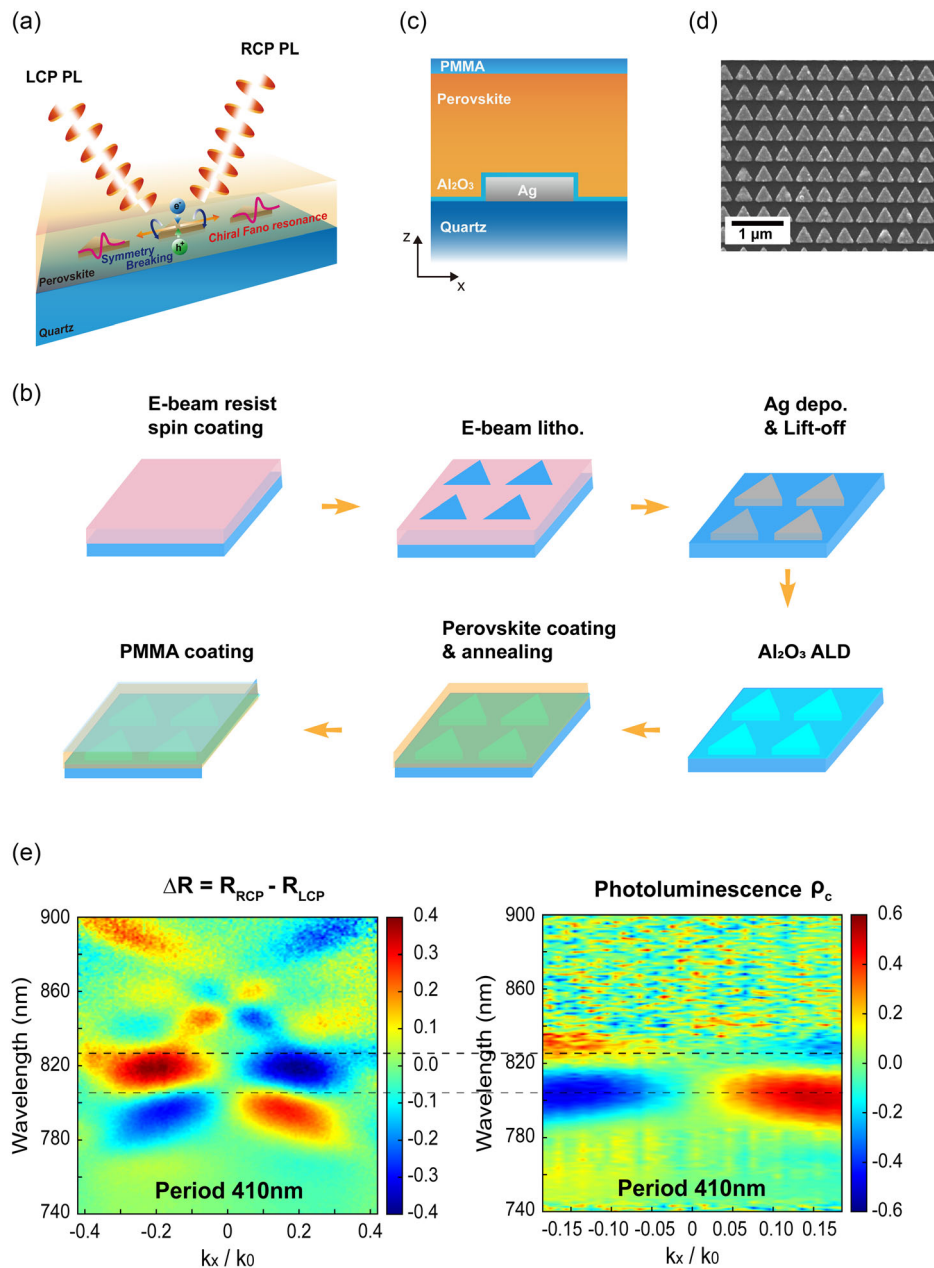


Figure 2. Chiral emission via chiral Fano resonances (extrinsic chirality). a) Schematic for the sample, where an organic-inorganic hybrid perovskite (MAPbI₃) is spin-coated on top of triangular silver patterns. b) Schematic for the fabrication procedure. c) Schematic for the sample side view. d) SEM image of the triangular silver patterns. e) Differential reflectance spectrum $\Delta R (= R_{RCP} - R_{LCP})$ and f) photoluminescence (PL) DCP ρ_c . Both ΔR and ρ_c show gradual changes with increasing periods. A clear correlation between ΔR and ρ_c is observed, together with a spectral offset between them. The horizontal dashed lines indicate the peak wavelengths of ρ_c . Note that the PL ρ_c spectrum becomes noisy beyond 820 nm because PL intensities become significantly weakened beyond 820 nm. Reproduced with permission.^[58] Copyright 2021, American Chemical Society.

Detailed theoretical analyses have revealed that a large difference in the field intensity under RCP and LCP light incidences is induced at the narrow-mode position of the chiral Fano resonances.^[91–96] The field enhancement of opposite helicity occurs at opposite angles. This chiral field enhancement leads to the directional coupling of chiral light emission in opposite directions, depending on the helicity of the light. The RCP and LCP components of the perovskite emission couple

into counter-propagating slab modes and eventually radiate at opposite angles in free space, resulting in high levels of chiral emission. The spectral features in the experiments can be further explained using the temporally coupled mode theory and causality relation of the lattice-dressed dipole polarizability.^[58]

Figure 3 displays two more recent experimental demonstrations of chiral emission from perovskite metasurfaces via

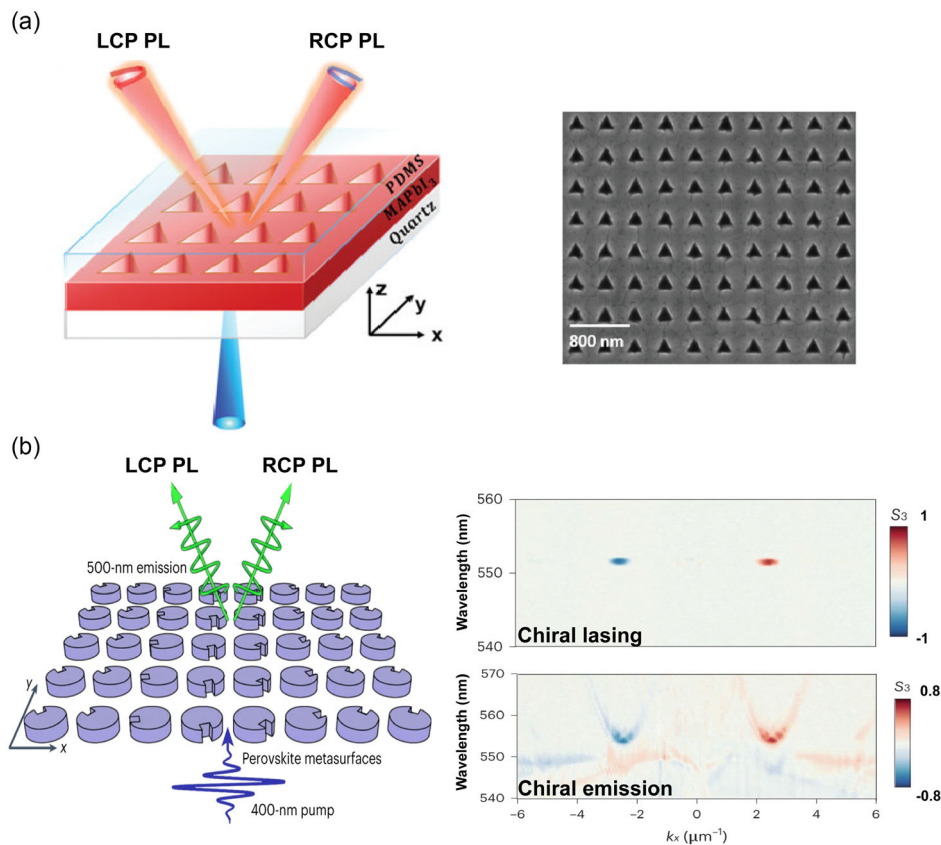


Figure 3. Chiral emission from perovskite metasurfaces via extrinsic chirality. a) Triangular hole patterns are created on a perovskite film (MAPbI_3). The broken in-plane inversion symmetry in the perovskite metasurface produces pairs of LCP and RCP PL in the opposite oblique directions, resulting in high levels of chiral emission ($\text{DCP} \approx 0.6$) at room temperature. Reproduced with permission.^[97] Copyright 2022, Wiley-VCH. b) Perovskite (FAPbBr_3) metasurfaces made on a patterned SiO_2 film. Photonic states with different spins at opposite valleys are created by geometric phases in the metasurface. Both chiral emission and chiral lasing are demonstrated in the same perovskite metasurface. Reproduced with permission.^[98] Copyright 2023, Springer Nature.

extrinsic chirality. The works in Figure 2 and 3 studied similar subjects and are complementary to each other. Therefore, we introduce them together in this section. In Figure 3a, an array of triangular holes was patterned on a 170 nm thick perovskite film (MAPbI_3) using nanoimprint lithography.^[97] The broken in-plane inversion symmetry in the perovskite metasurface produced pairs of LCP and RCP PL in opposite oblique directions, resulting in high levels of chiral emission ($\text{DCP} \approx 0.6$) at room temperature. In Figure 3b, a spin-valley-locked perovskite metasurface was used to generate chiral emissions at a large emission angle of 41° .^[98] The perovskite metasurface was fabricated by patterning photonic structures on SiO_2 and growing polycrystalline perovskites (FAPbBr_3) using a self-limiting assembly technique (see scanning electron microscopy image). The spin-dependent geometric phases in the metasurface were imparted into the bound states in the continuum (BICs) via Brillouin zone folding. This produced leaky photonic states with different spins in opposite valleys (producing pairs of RCP/LCP PL at two large opposite angles). Chiral lasing was also demonstrated using the same perovskite metasurface, resulting in a high DCP of 0.91 and a small beam-divergence angle of 1.6° .

2.2. Chiral Photoluminescence from Perovskite Metasurfaces Via Intrinsic Chirality

Chiral metasurfaces can significantly enhance chiral responses with unprecedented design flexibility. However, obtaining optimal chiral emission with near-unity DCP remains a challenge. Moreover, in extrinsic chiral metasurfaces, the RCP and LCP emissions are generated in pairs and emitted at two opposite oblique angles. Recently, chiral emission in the normal direction was demonstrated using a perovskite metasurface with planar chiral geometries without breaking the out-of-plane mirror symmetry.^[81] However, typical planar chiral metasurfaces (such as gammadions and z-shaped pattern arrays) generate opposite helicity of chiral emissions upward and downward, following the chiral response of planar intrinsic chirality. Therefore, the 3D intrinsic chirality with the maximum chiral response is desirable for high levels of chiral emission in the normal direction with the same helicity of chiral emissions upward and downward.

Objects with maximum chirality should interact strongly with one helicity of circular polarization and not interact with the other helicity. Moreover, the polarization state should remain

unchanged during this interaction; thus, the helicity of the incident fields should be preserved.^[99] Maximum chirality is important for maximizing chiral light-matter interactions. These chiral interactions can be implemented, e.g., using chiral BICs. Optical BICs are the eigenmodes embedded in a radiative continuum.^[100–108] BICs provide a new avenue for strong light confinement via symmetry mismatch or destructive interference and are a new platform for high-Q optical resonances and strong field enhancement. Recently, the concept of optical BICs has been extended to chiral resonances.^[28,109–116] Chiral BICs can be created by breaking the out-of-plane mirror symmetry of optical metasurfaces. Using chiral BICs, chiral interactions can be maximized for one helicity via critical coupling, while maintaining transparency for the other helicity. Maximum chirality via chiral BICs is highly desirable in the visible spectral range, where important applications of chiral emission exist. However, such 3D intrinsic chirality requires breaking the out-of-plane mirror symmetry, and its experimental realization is challenging.

Figure 4 displays an experimental demonstration of such chiral BICs and maximally chiral emission using perovskite metasurfaces.^[60] Chiral BICs are realized in the visible range by controlling the etching depth in the substrate and inducing out-of-plane symmetry breaking. An achiral perovskite layer (organic–inorganic hybrid perovskite layer, (PEA)₂PbI₄) was spin-coated onto a patterned glass substrate, followed by annealing and overcoating with a thick PMMA layer (Figure 4a). The perovskite layer has a higher refractive index than the surrounding medium (PMMA and quartz); thus, it forms a dielectric metasurface. The intrinsically chiral metasurface consists of a square lattice of paired rectangular bars. Chiral quasi-BICs can be created in such pairs of dielectric (perovskite) bars by adjusting the bar tilt angle θ and height difference D together (Figure 4b). This condition corresponds to antiparallel dipoles of the same magnitude with in-plane rotation θ and vertical offset d ($= D/2$), which satisfy $\theta \propto d$. The radiation of the antiparallel dipoles without an in-plane rotation or vertical offset nearly cancels out in the normal direction. However, by tilting the two dipoles outward with a proper vertical offset, a chiral quasi-BIC resonance can be induced. Figure 4c displays a comparison of the simulated field profiles in the normal incidence direction. A chiral response does not exist at a zero tilt angle. However, for the tilted bars (14°), the RCP field intensity is significantly enhanced, whereas the LCP field intensity is strongly suppressed, clearly indicating that extreme chiral responses exist in the metasurface.

In the experiment, grayscale electron-beam lithography was employed to control the etching depth in the substrate and induce out-of-plane symmetry breaking. Figure 4d displays the SEM images (top view) of the patterned resists after development, while Figure 4e shows the cross-sectional SEM image (side view) of the sample after quartz etching. The reflection and PL measurements clearly indicate the features of the chiral quasi-BICs in the visible spectral range. By properly adjusting the in-plane and out-of-plane symmetry breaking, chiral emission with an extremely high DCP (approaching 0.9) was demonstrated in the normal direction. Figure 4f displays the emission enhancement factors of the RCP and LCP emissions (red and blue curves, respectively) and corresponding DCP with varying tilt angles (green curve). Both the top and bottom emissions exhibit the same helicity, thereby confirming the 3D intrinsic chirality.

Maximally chiral emission can be understood from the reciprocity principle, which states that swapping the positions of the electromagnetic field source and detector does not change the physical situation. This implies that the far-field radiation power and polarization from an ensemble of randomly positioned and oriented dipolar emitters can be obtained by calculating the field enhancements at the dipole positions under incident light. The reciprocity principle ensures that the field enhancement calculation in the emission layer yields the same outcome as the dipole ensemble calculations. Compared with typical dipole simulations, reciprocity analysis simplifies emission calculations and provides insights into the optimal design of metasurfaces because field enhancement in optical nanostructures is more straightforward to understand and optimize than directly addressing randomly positioned dipole ensembles.

The Lorentz reciprocity principle states^[117,118] that for any two current densities $\mathbf{j}_{1,2}$

$$\int \mathbf{j}_1 \cdot \mathbf{E}_2 dV = \int \mathbf{j}_2 \cdot \mathbf{E}_1 dV \quad (1)$$

where $E_{1,2}$ is the electric fields produced by $\mathbf{j}_{1,2}$. For a dipole source \mathbf{p}_m , where $\mathbf{j}_m = -i\omega\mathbf{p}_m\delta(\mathbf{r} - \mathbf{r}_m)$ ($m = 1, 2$), this is simplified to

$$\mathbf{p}_1 \cdot \mathbf{E}_2(\mathbf{r}_1) = \mathbf{p}_2 \cdot \mathbf{E}_1(\mathbf{r}_2) \quad (2)$$

Therefore, using reciprocity, we can obtain the emission enhancement by calculating the field enhancement under an incident plane wave into a light-emitting medium.^[119–123] In chiral emission calculations, circularly polarized plane waves are incident on a perovskite metasurface at varying angles. By integrating the total electric field intensity in the perovskite region and normalizing it to the integrated field intensity in empty space, we can obtain the emission enhancement for each emission angle: \hat{I}_{RCP} and \hat{I}_{LCP} for the RCP and LCP incidences, respectively. Note that the hat notation for the enhancement factor indicates that it is a normalized quantity. Assuming that the light-emitting medium is achiral, the theoretical DCP is calculated as $\rho_c = (\hat{I}_{\text{RCP}} - \hat{I}_{\text{LCP}})/(\hat{I}_{\text{RCP}} + \hat{I}_{\text{LCP}})$.

Under incident circularly polarized light, chiral quasi-BICs can induce strong field enhancement for one helicity while decoupled from the other helicity, leading to high levels of chiral emission via reciprocity. From the temporal coupled mode theory, the field enhancement \hat{I} in an optical mode is related to the Q factors (or damping rates)^[124,125]

$$\hat{I} \propto \frac{Q^2}{Q_r} = \frac{\gamma_r}{(\gamma_r + \gamma_{\text{nr}})^2} \quad (3)$$

where $Q = \omega_0/2(\gamma_r + \gamma_{\text{nr}})$ and $Q_r = \omega_0/2\gamma_r$ are the total and radiative Q factors, respectively. Here γ_r and γ_{nr} are the radiative and nonradiative damping rates, respectively. We observe that the field enhancement (or emission enhancement) depends on the balance between the radiative and nonradiative damping rates. From $d\hat{I}/d\gamma_r = 0$, we find that the emission enhancement reaches a maximum at $\gamma_r = \gamma_{\text{nr}}$ (critical coupling). At this critical coupling condition, the maximum field enhancement is $\hat{I}_{\text{max}} \propto 1/\gamma_{\text{nr}}$. This implies that the maximum field enhancement (or emission enhancement) is ultimately limited by the nonradiative

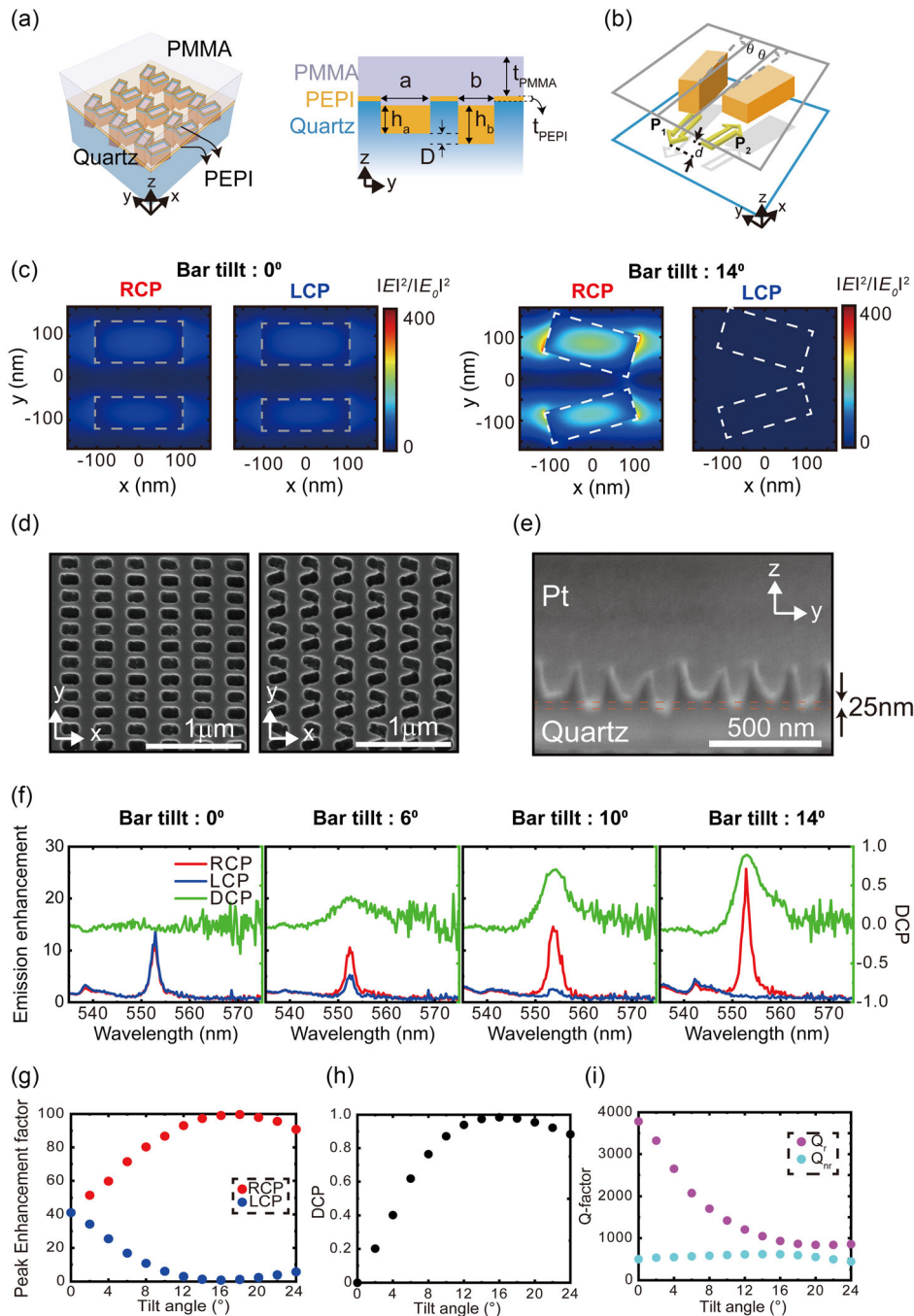


Figure 4. Maximally chiral emission via chiral quasi-bound states in the continuum (BICs) (intrinsic chirality). a) Sample schematic. Grayscale lithography is employed to control the etching depths in the substrate and induce out-of-plane symmetry breaking. b) The metasurface supporting a chiral quasi-BIC resonance consists of pairs of rectangular bars, which hold antiparallel dipoles with in-plane rotation θ and vertical offset d ($= D/2$, where D is the height difference between the two rectangular bars). c) Electric field intensities in the normal incidence direction for the bar tilt angles of 0° and 14° , which are measured in the middle plane of the bar pair. d) SEM image of patterned resists after development. e) SEM image of the cross-sectional view of the etched glass substrate showing a depth difference of $D \approx 25$ nm in the bar pair. f) Angle-resolved PL spectra for varying tilt angles in the normal direction ($k_x = 0$). At a tilt angle of 14° , RCP PL is strongly enhanced while LCP PL is strongly suppressed. Therefore, PL DCP reaches a near-unity value. g–i) Reciprocity calculations for gradually varying tilt angles at a fixed height difference of $D = 25$ nm. g) Peak enhancement factor, h) DCP, and i) Radiative and non-radiative Q factors obtained from numerical simulations. Reproduced with permission.^[60] Copyright 2023, Wiley-VCH.

damping rate (or absorption losses). Therefore, if an metasurface is defined by a light-emitting medium itself (as in Figure 4), the ultimate emission enhancement is limited by the absorption losses of the light-emitting medium.

Chiral emission with near-unity DCP ($|\rho_c| \rightarrow 1$) together with the maximized emission intensity can result from chiral quasi-BICs. Light-emitting perovskite metasurfaces that support chiral BICs can satisfy these two conditions almost at the same time. Note that it is important to achieve the high emission intensity as well as large DCP. Because the DCP is a ratio between the two emission intensities, it can be huge even when the actual emission intensities are negligibly small. From $\rho_c = (\hat{I}_{\text{RCP}} - \hat{I}_{\text{LCP}}) / (\hat{I}_{\text{RCP}} + \hat{I}_{\text{LCP}})$, the ideal chiral emission can be achieved when i) one helicity is decoupled from the outside (e.g., $\hat{I}_{\text{LCP}} \rightarrow 0$) and ii) the field intensity enhancement is maximized for the other helicity via critical coupling (e.g., $\hat{I}_{\text{RCP}} \rightarrow \text{maximum}$).

Figure 4g–i illustrate this case for a perovskite metasurface using numerical simulations.^[60] Figure 4g,h display how the peak enhancement factors for the RCP and LCP emissions and resulting DCP change with bar tilt angle. DCP is maximized around 14°–20°, reaching a near-unity value ($\rho_c \approx 0.98$). To directly investigate the critical coupling condition, the radiative and nonradiative damping rates (γ_r and γ_{nr} , respectively) and corresponding Q factors are extracted from the simulated absorptance spectra. Figure 4i displays how these two Q factors change with the tilt angle. As the bar tilt angle increases, the radiative Q factor (Q_r) decreases rapidly and approaches the nonradiative Q factor (Q_{nr}). Although they do not cross (meaning that the exact critical coupling does not arrive), they approach each other very closely around 14°–20°. This explains why the peak emission enhancement changes rather slowly and is maximized over a range of tilt angles.

2.3. Chiral Photoluminescence from Other Achiral Materials

Thus far, we have discussed chiral emission from metasurfaces and metacavities employing achiral perovskite materials. Similar chiral emission can be obtained by employing other achiral materials.^[126,127] Herein, we briefly introduce such demonstrations based on dielectric and plasmonic chiral nanostructures. **Figure 5a** displays chiral emission from conventional solid-state semiconductor materials.^[128] Chiral emission with a DCP of 0.26 at room temperature was demonstrated from InAs quantum dots embedded in a GaAs waveguide layer using dielectric chiral nanostructures (GaAs gammadions) on top. Similar semiconductor chiral nanostructures have also been used to produce chiral emission with a large DCP of ≈ 0.81 at a low temperature (5 K).^[129,130]

As shown in Figure 5b, plasmonic chiral nanostructures (e.g., silver nanorod pairs with a lateral shift) were used to generate chiral emission from achiral dye molecules via planar intrinsic chirality.^[131] An array of similar plasmonic particle pairs was also designed to excite surface lattice resonances,^[132] and chiral emission with a large DCP of ≈ 0.7 was obtained at oblique emission angles, even for the achiral geometry (i.e., with no lateral shift in the plasmonic particle pair) due to extrinsic chirality.

Chiral emission can also be generated from colloidal quantum dots.^[133–136] In Figure 5c, a planar metasurface consists of a periodic array of silicon pillar dimers with broken in-plane mirror

symmetry.^[133] A thin film of PbS/CdS quantum dots was coated on the silicon metasurface to generate chiral emission with a large DCP of 0.74 and strongly enhanced emission intensities. Chiral emission from quantum dots has also been demonstrated using plasmonic split ring resonant nanoantennas.^[134] The phase-locked interference of different multipolar moments resulted in chiral emission because the spin of the emitted photons was locked to their transverse momentum. A pair of RCP and LCP emissions was generated into the opposite halves of the symmetry plane of the achiral split-ring nanoantenna owing to extrinsic chirality.

Figure 5d,e displays chiral lasing from dielectric metasurfaces. In Figure 5d, the chiral emission and chiral lasing of dye molecules were demonstrated using intrinsic chirality in resonant metasurfaces.^[113] Instead of challenging out-of-plane symmetry breaking, tilted planar geometries were adopted to create high- Q chiral quasi-BICs with a giant field enhancement (i.e., realizing 3D intrinsic chirality). The same dielectric metasurface structure exhibited high DCP in both the spontaneous emission (i.e., chiral emission) and stimulated emission (i.e., chiral lasing) regimes. In Figure 5e, a dielectric metasurface was designed to manifest the photonic Rashba-type spin splitting of a BIC resonance.^[137] This produced opposite spin-polarized $\pm K$ valleys due to photonic spin-orbit interaction emerging under inversion symmetry breaking. The spin-valley resonant dielectric metasurface was combined with a 2D monolayer semiconductor (WS_2) to generate chiral lasing at the K valleys. In general, optical nanostructures can be used to control valley-polarized emission in 2D transition metal dichalcogenide (TMD) semiconductors.^[138–140] Refer to a recent review article for more details.^[141]

3. Chiral Electroluminescence

3.1. Chiral Electroluminescence from Perovskite Metacavities

Extensive studies have been conducted on chiral emission; however, the majority have been limited to PL. A chiral EL with substantial DCP is more desirable for device applications. **Figure 6** displays such a chiral EL device based on a new concept of “thin-film chiral metacavity”.^[62] A layer of achiral perovskite (CsPbBr_3) is confined between a metal and metasurface mirror (“metamirror”) created by an array of triangular silicon particles. A polycrystalline silicon layer with broken inversion symmetry is integrated into the thin-film EL device (Figure 6a). The bottom silicon and top metal layers form a Fabry–Pérot cavity that confines the optical fields internally. The bottom silicon pattern supports nonlocal (or spatially extended) resonant modes (leaky Bloch modes)^[142–144] and functions as a chiral metamirror. With this bottom layer, the resonance condition of the Fabry–Pérot resonance is significantly modified owing to the rapid phase change near the narrowband Bloch modes. The inversion symmetry-broken (triangular) patterns induce strong chiral responses at oblique incidence (or emission) angles near the emission band (≈ 520 nm) of CsPbBr_3 . The eigenstate polarization of the triangular silicon layer is close to the ideal circular polarization; thus, strong chiral responses can be achieved over a wide range of incidence angles.

In this Fabry–Pérot cavity, both the bottom triangular silicon pattern and top metal mirror reverse the helicity of the circular polarization upon reflection. Therefore, field enhancement

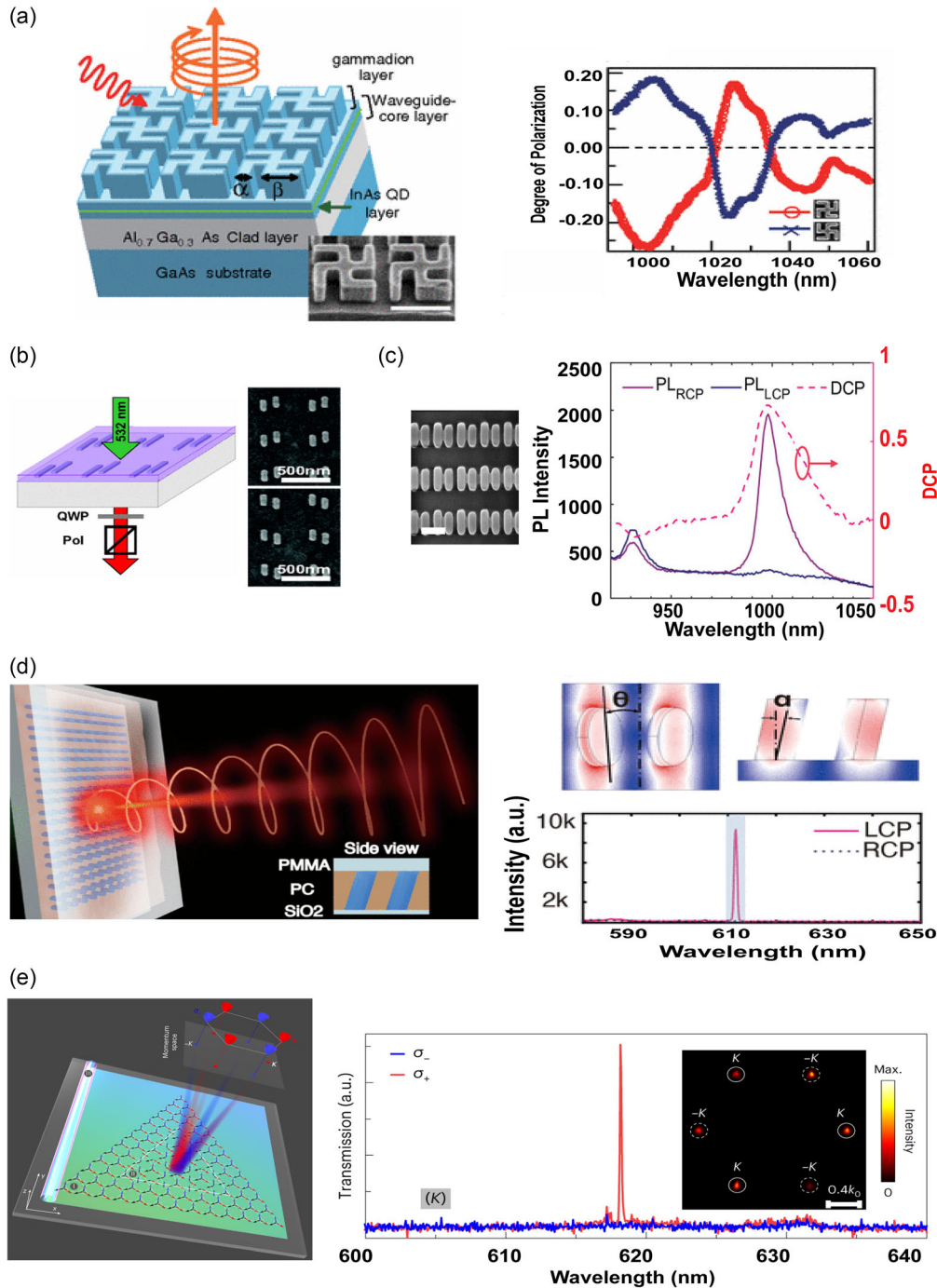


Figure 5. Chiral emission from other achiral materials. a) InAs quantum dots with dielectric chiral nanostructures on top. Reproduced with permission.^[128] Copyright 2011, American Physical Society, licensed under a Creative Commons Attribution 3.0 License. b) Dye molecules with plasmonic chiral metasurfaces. Reproduced with permission.^[131] Copyright 2013, American Physical Society. c) Colloidal quantum dots with a planar dielectric metasurface. Reproduced with permission.^[133] Copyright 2023, Wiley-VCH. d) Chiral lasing in dye molecules is achieved via 3D intrinsic chiral BICs. Reproduced with permission.^[113] Copyright 2022, The American Association for the Advancement of Science. e) Chiral lasing is achieved via photonic Rashba-type spin splitting in a 2D monolayer semiconductor. Reproduced with permission.^[137] Copyright 2023, Springer Nature.

occurs inside the cavity (similar to a conventional cavity), while strong chiral responses are induced at oblique angles. A broad Fabry–Pérot resonance and narrow Bloch modes are spectrally overlapped in the optimized device geometry, and the emission

properties are significantly modified. The chiral Fabry–Pérot modes supported by this metacavity determine the asymmetry of the EL, and pairs of LCP and RCP EL of equal powers are generated in opposite oblique directions.

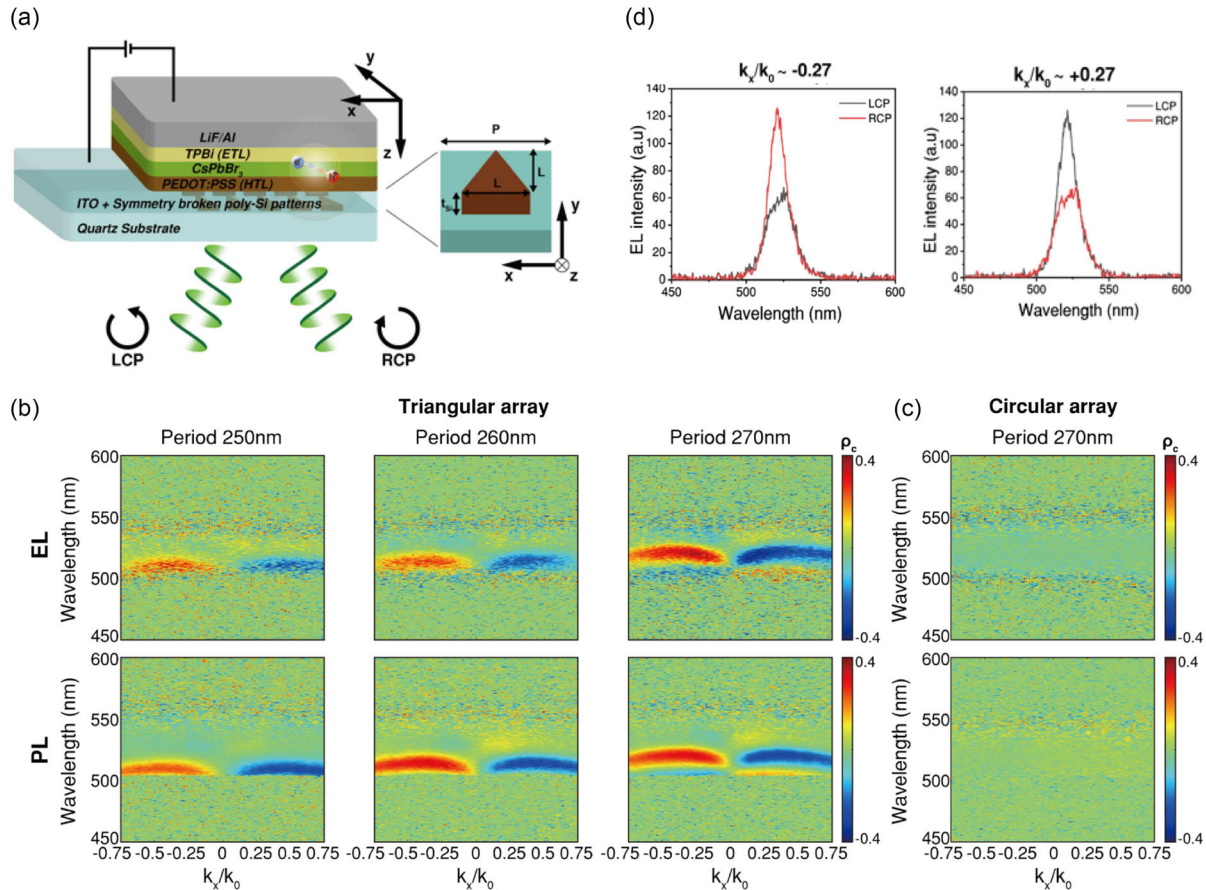


Figure 6. Chiral electroluminescence (EL) device based on a thin-film chiral metacavity. a) Schematic of the simulation configuration. $L = 200$ nm, $t_{\text{Si}} = 40$ nm, $t_{\text{ITO}} = 60$ nm, $t_{\text{HTL}} = 35$ nm, $t_{\text{perovskite}} = 45$ nm, $t_{\text{res}} = 20$ nm, and $t_{\text{ETL}} = 30$ nm. b) EL and PL degree of circular polarization (DCP) for the triangular pattern of the different pattern periods (250–270 nm). Both EL and PL spectra show similar behavior. c) EL and PL DCP for the circular pattern (period 270 nm). d) EL line spectra and the corresponding DCP at $k_x/k_0 = -0.27$ (or $\theta = -15.7^\circ$) and $k_x/k_0 = +0.27$ (or $\theta = +15.7^\circ$), respectively. The peak EL DCP reaches ≈ 0.38 . Reproduced with permission.^[62] Copyright 2023, The American Association for the Advancement of Science, licensed under a Creative Commons Attribution NonCommercial License 4.0 (CC BY-NC).

Figure 6b displays a comparison of the measured EL and PL spectra for different pattern periods (250–270 nm). It presents the emission spectra as a function of wavelength λ_0 and in-plane wavevector k_x/k_0 . Both the EL and PL spectra exhibit a clear chiral response, and the chiral emission band gradually redshifts with an increasing pattern period. It demonstrates that the EL and PL spectra exhibit the same chiral responses. In contrast, the EL and PL spectra from the inversion-symmetric (circular) pattern do not exhibit such chiral responses (Figure 6c). This confirms that a large chiral response is generated by the inversion-symmetry-broken (triangular) pattern and that the chiral emission originates from the chiral behavior of the cavity resonance. Figure 6d shows the EL line spectra at negative and positive angles ($k_x/k_0 = -0.27$ and $k_x/k_0 = +0.27$ at period 270 nm). The LCP EL intensity is higher for $k_x < 0$, whereas the RCP EL intensity is higher for $k_x > 0$. The EL spectrum manifests a substantial DCP at room temperature; the peak DCP reaches $\rho_c \approx 0.38$.

The chiral response of the metamirror can be understood from the chiral coupled-mode theory and multipole expansion

analysis. From these analyses, it is found that the close-to-maximum extrinsic chirality in the inversion-symmetry-broken mirror results from the interplay of three dipole moments: two electric dipoles (P_x and P_y) and one magnetic dipole (M_z).

From the metamirror characteristics, we can obtain analytical expressions for the field intensities inside the metacavity and evaluate the field enhancement factors.^[62] By reciprocity, these chiral field enhancements are directly related to the chiral emission. Both the bottom metamirror and top metal mirror reverse the helicity of the incident circularly polarized light by reflection while the metamirror transmits preserving the helicity. Consequently, the cavity modes of opposite handedness remain uncoupled. The LCP and RCP field enhancements in the chiral metacavity can be expressed by the following two independent modes

$$\frac{I_{\text{LCP}}^{\text{inc}}}{I_0} \propto \frac{|t_{\text{LL}}|^2}{|1 - r_{\text{LR}} r_{\text{metal}} e^{2ik_z d}|^2}, \quad \frac{I_{\text{RCP}}^{\text{inc}}}{I_0} \propto \frac{|t_{\text{RR}}|^2}{|1 - r_{\text{LR}} r_{\text{metal}} e^{2ik_z d}|^2} \quad (4)$$

where r_{metal} is the reflection coefficient of the metal mirror and k_z is the vertical wavevector component. The chiral asymmetry of the

field enhancement and the high DCP of the EL can be understood from this equation. This analytical equation further reveals a different type of interplay between the resonant and background reflections from the metamirror, depending on the cavity thickness. These analyses elucidate the design strategies for compact chiral EL devices that can simultaneously enhance both chiral emission intensity and DCP.

This approach to chiral EL generation is based on the optical mode properties of a metacavity with symmetry-broken patterns. Therefore, chiral emission properties can be tailored by optimizing the pattern geometry and dimensions. In this metacavity design with triangular patterns, the LCP and RCP emissions are clearly separated into two well-defined directions ($k_x < 0$ and $k_x > 0$). As numerous chiral applications require chiral light beams of both helicities, this design can be useful for innovative device integration and applications requiring ultracompact chiral light sources. Moreover, this scheme is applicable to other achiral materials. Chiral EL with substantial DCP can be obtained from achiral emitters without special spin injection or filters.^[145–148]

3.2. Chiral Electroluminescence from Other Achiral Materials

As stated previously, most chiral emission studies based on metasurfaces and metacavities have been limited to chiral PL demonstrations. However, there have been several relevant reports recently. In Ref. [149], electrically driven chiral lasing has been demonstrated using chiral nanostructures at a low temperature (1.8 K). A chiral photonic crystal slab structure was integrated on top of an electrically pumped semiconductor microcavity, where active quantum wells were placed between *p*-doped and *n*-doped distributed Bragg reflectors (DBRs). In the spontaneous emission regime (chiral emission), the EL DCP was relatively low ($\rho_c \approx 0.1$). However, in the coherent lasing regime (chiral lasing), the EL DCP was increased to $\rho_c \approx 0.9$. Recently, chiral EL was also demonstrated in an organic single-crystal microcavity, which included a 990 nm thick birefringent organic crystal [1,4-bis((E)-2,4-dimethylstyryl)-2,5-dimethylbenzene (6M-DSB)].^[150] Although this work did not involve an optical metasurface or metacavity, chiral EL with a large peak DCP of 0.55 was demonstrated at room temperature using the photonic spin–orbit interaction in a birefringent organic single crystal.

Table 1 summarizes different approaches for chiral emission from various *achiral* emitters. The table is grouped into two sections (chiral PL and EL) and compares key aspects in the recent studies of chiral emission. Table 1 also includes the data from 2D TMD semiconductor devices.^[151,152] Although metasurfaces or metacavities were not employed in these studies, chiral emission was generated from achiral materials, and thus these works can be compared with the metasurface or metacavity approach. For the general emission characteristics of *chiral* emitters, refer to a recent review on chiral materials.^[57]

4. Conclusion and Outlook

We reviewed the recent progress in chiral emission from optical metasurfaces and metacavities, considering both chiral PL and EL of achiral emitters. Chiral light sources with near-unity DCP and strong emission intensities are desirable for important

applications. This review provides physical insights into ideal chiral emission generation using reciprocity and critical coupling. The light emission problem is converted into the field enhancement calculation under light incidence using the Lorentz reciprocity principle. Equation (1) and (2) explained the general reciprocity principle. The descriptions relevant to Equation (3) and Figure 4g–i explain how critical coupling can be used to optimize chiral emission. The descriptions relevant to Figure 4b,c explain how to design the chiral BIC metasurface to realize such ideal chiral emission. Chiral quasi-BICs can induce strong field enhancement for one helicity of circular polarization while the field enhancement for the other helicity is strongly suppressed, leading to high levels of chiral emission via reciprocity. The descriptions relevant to Equation (4) explained the optimization procedure for chiral EL in chiral metacavities.

Finally, possible future directions for this subject are discussed. Optical coupling to the extended leaky modes enhances the spatial coherence of the emission fields.^[112,153–155] Therefore, properly designed metasurfaces can enable direct chiral emission with tailored wavefronts without employing bulky optical elements. Chiral emission, which is normally incoherent, could be made directional or focused by coupling it to extended optical modes. This opens interesting new opportunities for the development of highly functional and compact light sources.

The concept of the chiral Fabry–Pérot cavity demonstrated in Figure 6 can be extended to single-handed chiral metacavities. The thin-film chiral cavity, displayed in Figure 6, has a metamirror on the bottom plane only. If both top and bottom planes are made of chiral metamirrors that reflect light only with a specific helicity of circular polarization, single-handed chiral metacavities having strong field enhancement only for one helicity (RCP or LCP) can be constructed. These chiral cavities can exhibit highly enhanced chiral PL and EL in the normal direction.^[156,157] They can also be used in constructing a single-handed electrically driven chiral laser.

Chiral emission in strong-coupling regimes comprises another interesting future research direction. Excitons in luminescent materials and resonant photonic modes in an optical cavity can form hybrid light-matter states called exciton polaritons.^[158–165] In a recent study,^[59,166] circularly polarized eigenstates derived from optical BICs were used to generate chiral emission from perovskite polariton metasurfaces with a large DCP exceeding 0.8. Optical BICs are topological in nature and can be described by robust topological charges in momentum space. Circularly polarized eigenstates induced from BICs via symmetry breaking correspond to topological half-charges. Therefore, the momentum space topology can be utilized to manipulate chiral polariton emission and lasing based on the topological charge concept.^[167–170]

Exciton polaritons combine luminescent materials with resonant optical structures to form a single entity. Therefore, chiral light-emitting metasurfaces and metacavities are promising platforms for studying and exploiting chiral interactions in exciton polaritons. The chiral cavity structure displayed in Figure 6 employs polycrystalline silicon nanopatterns as the bottom metamirror. However, the absorption losses of polycrystalline patterns are a limiting factor for cavity field enhancement. If a dielectric structure with no (or reduced) absorption losses can be introduced (e.g., using GaP), both the emission intensity

Table 1. Comparison of chiral emission from achiral emitters.

Emission Type	DCP	Emitter	Approach for chiral emission generation	Temp.	Ref.
Chiral PL	0.524	Perovskite (MAPbI ₃)	Extrinsic chiral metasurface	Room temp.	[58]
Chiral PL	0.835	Perovskite [(PEA) ₂ PbI ₄]	Extrinsic chiral BIC metasurface	Room temp.	[59]
Chiral PL	0.6	Perovskite (MAPbI ₃)	Extrinsic chiral metasurface	Room temp.	[97]
Chiral PL and lasing	0.66 (Chiral PL) 0.91 (chiral lasing)	Perovskite (FAPbBr ₃)	Extrinsic chiral metasurface (optical pumped lasing)	Room temp.	[98]
Chiral PL	0.15	Perovskite nanocrystal (CsPbBr ₃)	Planar intrinsic chiral metasurface	Room temp.	[81]
Chiral PL	0.9	Perovskite [(PEA) ₂ PbI ₄]	3D intrinsic chiral metasurface	Room temp.	[60]
Chiral PL	≈0.1	dye molecule	Silver nanorod pair (planar intrinsic chiral)	Room temp.	[131]
Chiral PL	0.7 (at an oblique angle for achiral geometry)	dye molecule	Array of plasmonic particle pairs (extrinsic & planar intrinsic)	Room temp.	[132]
Chiral PL and lasing	0.989 (chiral lasing)	dye molecule	3D intrinsic chiral metasurface	Room temp.	[113]
Chiral PL	0.9	dye molecule	3D intrinsic chiral metasurface	Room temp.	[115]
Chiral PL	0.26	InAs QD	Planar intrinsic chiral metasurface	Room temp.	[128]
Chiral PL	0.81	InAs QD	Structured chiral planar microcavity	5 K	[129]
Chiral PL	0.81	InAs QD	Chiral photonic crystal slab	5 K	[130]
Chiral PL	0.17	CdSe/ZnS QD	Plasmonic planar intrinsic chiral metasurface	Room temp.	[135]
Chiral PL	0.74	PbS/CdS QD	Planar intrinsic chiral metasurface	Room temp.	[133]
Chiral PL	0.88	TMD (WS ₂)	Extrinsic chiral BIC metasurface	Room temp.	[139]
Chiral lasing	≈1	TMD (WS ₂)	photonic Rashba-type spin splitting of a BIC resonance (extrinsic, optically pumped lasing)	Room temp.	[137]
Chiral EL	0.45	TMD (WSe ₂)	Electric double-layer transistor	40 K	[151]
Chiral EL	≈0.07	TMD (WS ₂)	Strained monolayer TMD	280 K	[152]
Chiral EL	0.55	Organic single crystal (990 nm-thick 6M-DSB)	Photonic spin-orbit interaction in a birefringent organic single crystal	Room temp.	[150]
Chiral EL and lasing	0.1 (chiral EL) 0.9 (chiral lasing)	GaAs quantum well	Chiral photonic crystal slab on top of a microcavity (electrically pumped lasing)	1.8 K	[149]
Chiral EL	0.38	Perovskite (CsPbBr ₃)	Extrinsic chiral metacavity	Room temp.	[62]

and DCP can be significantly enhanced. More importantly, if the helicity-dependent chiral field intensity in the cavity increases further, strong coupling in chiral cavities can be realized at room temperature. Such chiral cavities in the strong-coupling regime can enable the formation of chiral polariton states with helicity-dependent vacuum Rabi splitting's.^[171,172] This provides interesting opportunities for the development of spin-based active optical devices.

Owing to their excitonic components, exciton polaritons exhibit strong nonlinearity, which can be exploited for active devices (such as optical switches and logic gates).^[173–175] The bosonic nature of exciton polaritons also makes them interesting for quantum phenomena such as polariton condensation, lasing, and superfluidity.^[176–178] Exciton polaritons also hold promise for use in quantum simulations.^[179] Particularly, polariton interactions are maximized when they have the same spin polarization.^[180,181] Therefore, strongly enhanced helicity-dependent fields in chiral cavities may help increase the interactions between spin-polarized exciton polaritons. This approach can be exploited in future polariton devices and quantum simulators.

In this review, we have focused on the chiral emission from achiral emitters. However, it could also be interesting to study the interactions between chiral molecules (or materials) and chiral metasurfaces/metacavities in the weak and strong coupling regimes. These studies can further enhance the control of chiral responses and may lead to applications in novel light sources, optical sensors, and active functional elements.

Acknowledgements

The authors acknowledge the support from National Research Foundation (NRF) of Korea (Grant Nos. NRF-2023R1A2C1004674 and 2022M3H4A1A04096465). This research was partially supported by Korea Institute for Advancement of Technology (KIAT) grant funded by the Korea Government (MOTIE) (P0023703, HRD Program for Industrial Innovation).

Conflict of Interest

The authors declare no conflict of interest.

Keywords

achiral emitters, chiral emission, electroluminescence, metasurfaces and metacavities, photoluminescence

Received: April 8, 2024
Revised: June 19, 2024
Published online:

- [1] S. Mason, *Trends Pharmacol. Sci.* **1986**, 7, 20.
- [2] D. Kondepudi, R. Hegstrom, *Sci. Am* **1990**, 262, 108.
- [3] J. Bailey, A. Chrysostomou, J. Hough, T. Gledhill, A. McCall, S. Clark, F. Ménard, M. Tamura, *Science* **1998**, 281, 672.
- [4] D. K. Kondepudi, D. J. Durand, *Chirality* **2001**, 13, 351.
- [5] L. D. Barron, in *Molecular Light Scattering And Optical Activity*, Cambridge University Press, Cambridge, England **2009**.
- [6] S. Boriskina, N. I. Zheludev, in *Singular And Chiral Nanoplasmonics*, Pan Stanford Publishing, Singapore, **2014**.
- [7] M. Schäferling, *Chiral Nanophotonics*, Springer, Cham, Switzerland **2017**.
- [8] M. Hentschel, M. Schäferling, X. Duan, H. Giessen, N. Liu, *Sci. Adv.* **2017**, 3, e1602735.
- [9] J. T. Collins, C. Kuppe, D. C. Hooper, C. Sibilina, M. Centini, V. K. Valev, *Adv. Opt. Mater.* **2017**, 5, 1700182.
- [10] Y. Luo, C. Chi, M. Jiang, R. Li, S. Zu, Y. Li, Z. Fang, *Adv. Opt. Mater.* **2017**, 5, 1700040.
- [11] J. Mun, M. Kim, Y. Yang, T. Badloe, J. Ni, Y. Chen, C.-W. Qiu, J. Rho, *Light Sci. Appl.* **2020**, 9, 139.
- [12] Y. Chen, W. Du, Q. Zhang, O. Avalor-Ovando, J. Wu, Q.-H. Xu, N. Liu, H. Okamoto, A. O. Govorov, Q. Xiong, C.-W. Qiu, *Nat. Rev. Phys.* **2022**, 4, 113.
- [13] A. Lininger, G. Palermo, A. Guglielmelli, G. Nicoletta, M. Goel, M. Hinczewski, G. Strangi, *Adv. Mater.* **2023**, 35, 2107325.
- [14] E. Plum, V. Fedotov, N. Zheludev, *J. Opt. A: Pure Appl. Opt.* **2009**, 11, 074009.
- [15] B. M. Maoz, A. Ben Moshe, D. Vestler, O. Bar-Elli, G. Markovich, *Nano Lett.* **2012**, 12, 2357.
- [16] K. Koshelev, Y. Tang, Z. Hu, I. I. Kravchenko, G. Li, Y. Kivshar, *ACS Photonics* **2023**, 10, 298.
- [17] J. K. Gansel, M. Thiel, M. S. Rill, M. Decker, K. Bade, V. Saile, G. V. Freymann, S. Linden, M. Wegener, *Science* **2009**, 325, 1513.
- [18] S. Zhang, J. Zhou, Y.-S. Park, J. Rho, R. Singh, S. Nam, A. K. Azad, H.-T. Chen, X. Yin, A. J. Taylor, X. Zhang, *Nat. Commun.* **2012**, 3, 942.
- [19] X. Yin, M. Schäferling, B. Metzger, H. Giessen, *Nano Lett.* **2013**, 13, 6238.
- [20] M. Decker, M. Ruther, C. E. Kriegler, J. Zhou, C. M. Soukoulis, S. Linden, M. Wegener, *Opt. Lett.* **2009**, 34, 2501.
- [21] A. Kuzyk, R. Schreiber, Z. Fan, G. Pardatscher, E.-M. Roller, A. Högele, F. C. Simmel, A. O. Govorov, T. Liedl, *Nature* **2012**, 483, 311.
- [22] S. Vignolini, N. A. Yufa, P. S. Cunha, S. Guldin, I. Rushkin, M. Stefik, K. Hur, U. Wiesner, J. J. Baumberg, U. Steiner, *Adv. Mater.* **2012**, 24, OP23.
- [23] S. Zanotto, G. Mazzamuto, F. Riboli, G. Biasiol, G. C. La Rocca, A. Tredicucci, A. Pianti, *Nanophotonics* **2019**, 8, 2291.
- [24] S.-D. Liu, J.-Y. Liu, Z. Cao, J.-L. Fan, D. Lei, *Nanophotonics* **2020**, 9, 3419.
- [25] J. Dixon, M. Lawrence, D. R. Barton III, J. Dionne, *Phys. Rev. Lett.* **2021**, 126, 123201.
- [26] J. Yang, H. Hu, Q. Zhang, S. Zu, W. Chen, H. Xu, *Nanophotonics* **2024**, 13, 357.
- [27] S. Wang, Z.-L. Deng, Y. Wang, Q. Zhou, X. Wang, Y. Cao, B.-O. Guan, S. Xiao, X. Li, *Light Sci. Appl.* **2021**, 10, 24.
- [28] T. Shi, Z.-L. Deng, G. Geng, X. Zeng, Y. Zeng, G. Hu, A. Overvig, J. Li, C.-W. Qiu, A. Alù, Y. S. Kivshar, X. Li, *Nat. Commun.* **2022**, 13, 4111.
- [29] Z.-Q. Wang, F.-J. Li, Q.-M. Deng, Z. Wan, X. Li, Z.-L. Deng, *Chin. Opt. Lett.* **2024**, 22, 023601.
- [30] S. Krasikov, A. Tranter, A. Bogdanov, Y. Kivshar, *Opto-Electron. Adv.* **2022**, 5, 210147.
- [31] X. Zhang, T. J. Cui, *Opto-Electron. Adv.* **2023**, 6, 230057.
- [32] E. Hendry, T. Carpy, J. Johnston, M. Popland, R. V. Mikhaylovskiy, A. J. Laphorn, S. M. Kelly, L. D. Barron, N. Gadegaard, M. Kadodwala, *Nat. Nanotechnol.* **2010**, 5, 783.
- [33] D. Leung, S. O. Kang, E. V. Anslyn, *Chem. Soc. Rev.* **2012**, 41, 448.
- [34] J. Kumar, H. Eraña, E. López-Martínez, N. Claes, V. F. Martín, D. M. Solís, S. Bals, A. L. Cortajarena, J. Castilla, L. M. Liz-Marzán, *Proc. Natl. Acad. Sci. USA* **2018**, 115, 3225.
- [35] T. Kakkar, C. Keijzer, M. Rodier, T. Bukharova, M. Taliany, A. J. Love, J. J. Milner, A. S. Karimullah, L. D. Barron, N. Gadegaard, A. J. Laphorn, M. Kadodwala, *Light Sci. Appl.* **2020**, 9, 195.
- [36] J. Feis, D. Beutel, J. Köpfler, X. Garcia-Santiago, C. Rockstuhl, M. Wegener, I. Fernandez-Corbaton, *Phys. Rev. Lett.* **2020**, 124, 033201.
- [37] W. Li, Z. J. Coppens, L. V. Besteiro, W. Wang, A. O. Govorov, J. Valentine, *Nat. Commun.* **2015**, 6, 8379.
- [38] P. Lodahl, S. Mahmoodian, S. Stobbe, A. Rauschenbeutel, P. Schneeweiss, J. Volz, H. Pichler, P. Zoller, *Nature* **2017**, 541, 473.
- [39] H. Hübener, U. D. D. Giovannini, C. Schäfer, J. Andberger, M. Ruggenthaler, J. Faist, A. Rubio, *Nat. Mater.* **2021**, 20, 438.
- [40] V. V. Tuchin, L. V. Wang, D. A. Zimnyakov, in *Optical Polarization In Biomedical Applications*, Vol. 467, Springer, Berlin **2006**.
- [41] D.-Y. Kim, *J. Korean Phys. Soc.* **2006**, 49, 505.
- [42] C. D. Stanciu, F. Hansteen, A. V. Kimel, A. Kirilyuk, A. Tsukamoto, A. Itoh, T. Rasing, *Phys. Rev. Lett.* **2007**, 99, 047601.
- [43] R. Farschi, M. Ramsteiner, J. Herfort, A. Tahraoui, H. T. Grahn, *Appl. Phys. Lett.* **2011**, 98.
- [44] Y. Yang, R. C. Da Costa, M. J. Fuchter, A. J. Campbell, *Nat. Photonics* **2013**, 7, 634.
- [45] S. H. Lee, S.-H. Lee, S.-U. Kim, S. Kang, S.-D. Lee, *Opt. Express* **2019**, 27, 11661.
- [46] J. Han, S. Guo, H. Lu, S. Liu, Q. Zhao, W. Huang, *Adv. Opt. Mater.* **2018**, 6, 1800538.
- [47] D.-W. Zhang, M. Li, C.-F. Chen, *Chem. Soc. Rev.* **2020**, 49, 1331.
- [48] Y. Deng, M. Wang, Y. Zhuang, S. Liu, W. Huang, Q. Zhao, *Light Sci. Appl.* **2021**, 10, 76.
- [49] G. Long, R. Sabatini, M. I. Saidaaminoy, G. Lakhwani, A. Rasmita, X. Liu, E. H. Sargent, W. Gao, *Nat. Rev. Mater.* **2020**, 5, 423.
- [50] J. Ma, H. Wang, D. Li, *Adv. Mater.* **2021**, 33, 2008785.
- [51] J. Ahn, E. Lee, J. Tan, W. Yang, B. Kim, J. Moon, *Mater. Horiz.* **2017**, 4, 851.
- [52] G. Long, C. Jiang, R. Sabatini, Z. Yang, M. Wei, L. N. Quan, Q. Liang, A. Rasmita, M. Askerka, G. Walters, X. Gong, J. Xing, X. Wen, R. Quintero-Bermudez, H. Yuan, G. Xing, X. R. Wang, D. Song, O. Voznyy, M. Zhang, S. Hoogland, W. Gao, Q. Xiong, *Nat. Photonics* **2018**, 12, 528.
- [53] J. Ma, C. Fang, C. Chen, L. Jin, J. Wang, S. Wang, J. Tang, D. Li, *ACS Nano* **2019**, 13, 3659.
- [54] A. Dey, J. Ye, A. De, E. Debroye, S. K. Ha, E. Bladt, A. S. Kshirsagar, Z. Wang, J. Yin, Y. Wang, R. L. Z. Hoye, L. Polavarpu, *ACS Nano* **2021**, 15, 10775.
- [55] C. Ye, J. Jiang, S. Zou, W. Mi, Y. Xiao, *J. Am. Chem. Soc.* **2022**, 144, 9707.
- [56] O. Graydon, *Nat. Photonics* **2023**, 17, 216.
- [57] F. Furlan, J. M. Moreno-Naranjo, N. Gasparini, S. Feldmann, J. Wade, M. J. Fuchter, *Nat. Photonics* **2024**, 18, 658.

- [58] I. C. Seo, Y. Lim, S.-C. An, B. H. Woo, S. Kim, J. G. Son, S. Yoo, Q.-H. Park, J. Y. Kim, Y. C. Jun, *ACS Nano* **2021**, *15*, 13781.
- [59] S. Kim, B. H. Woo, S.-C. An, Y. Lim, I. C. Seo, D.-S. Kim, S. Yoo, Q.-H. Park, Y. C. Jun, *Nano Lett.* **2021**, *21*, 10076.
- [60] Y. Lim, I. C. Seo, S.-C. An, Y. Kim, C. Park, B. H. Woo, S. Kim, H.-R. Park, Y. C. Jun, *Laser Photonics Rev.* **2023**, *17*, 2200611.
- [61] Y. Lim, I. C. Seo, Y. C. Jun, *Curr. Opt. Photon.* **2023**, *7*, 147.
- [62] S. Kim, S.-C. An, Y. Kim, Y. S. Shin, A. A. Antonov, I. C. Seo, B. H. Woo, Y. Lim, M. V. Gorkunov, Y. S. Kivshar, J. Y. Kim, Y. C. Jun, *Sci. Adv.* **2023**, *9*, eadh0414.
- [63] T. Ishihara, *J. Lumin.* **1994**, *60–61*, 269.
- [64] S. Zhang, P. Audebert, Y. Wei, A. Al Choueiry, G. Lanty, A. Bréhier, L. Galmiche, G. Clavier, C. Boissière, J.-S. Lauret, E. Deleporte, *Materials* **2010**, *3*, 3385.
- [65] B. R. Sutherland, E. H. Sargent, *Nat. Photonics* **2016**, *10*, 295.
- [66] S. A. Veldhuis, P. P. Boix, N. Yantara, M. Li, T. C. Sum, N. Mathews, S. G. Mhaisalkar, *Adv. Mater.* **2016**, *28*, 6804.
- [67] W. Li, Z. Wang, F. Deschler, S. Gao, R. H. Friend, A. K. Cheetham, *Nat. Rev. Mater.* **2017**, *2*, 1.
- [68] M. D. Smith, B. A. Connor, H. I. Karunadasa, *Chem. Rev.* **2019**, *119*, 3104.
- [69] X.-K. Liu, W. Xu, S. Bai, Y. Jin, J. Wang, R. H. Friend, F. Gao, *Nat. Mater.* **2021**, *20*, 10.
- [70] T.-H. Han, K. Y. Jang, Y. Dong, R. H. Friend, E. H. Sargent, T.-W. Lee, *Nat. Rev. Mater.* **2022**, *7*, 757.
- [71] K. Chen, Q. Zhang, Y. Liang, J. Song, C. Li, S. Chen, F. Li, Q. Zhang, *Front. Phys.* **2024**, *19*, 23502.
- [72] H. Dong, C. Ran, W. Gao, M. Li, Y. Xia, W. Huang, *eLight* **2023**, *3*, 3.
- [73] K. Liao, X. Hu, Y. Cheng, Z. Yu, Y. Xue, Y. Chen, Q. Gong, *Adv. Opt. Mater.* **2019**, *7*, 1900350.
- [74] M. Zhou, J. S. Sarmiento, C. Fei, X. Zhang, H. Wang, *J. Phys. Chem. Lett.* **2020**, *11*, 1502.
- [75] E. Hecht, *Optics*, Addison-Wesley, San Francisco, CA **2002**.
- [76] W. R. Kitzmann, J. Freudenthal, A.-P. M. Reponen, Z. A. VanOrman, S. Feldmann, *Adv. Mater.* **2023**, *35*, 2302279.
- [77] B. Gholipour, G. Adamo, D. Cortecchia, H. N. S. Krishnamoorthy, M. D. Birowosuto, N. I. Zheludev, C. Soci, *Adv. Mater.* **2017**, *29*, 1604268.
- [78] E. Y. Tiguntseva, D. G. Baranov, A. P. Pushkarev, B. Munkhbat, F. Komissarenko, M. Franckevicius, A. A. Zakhidov, T. Shegai, Y. S. Kivshar, S. V. Makarov, *Nano Lett.* **2018**, *18*, 5522.
- [79] A. S. Berestennikov, P. M. Voroshilov, S. V. Makarov, Y. S. Kivshar, *Appl. Phys. Rev.* **2019**, *6*, 031307.
- [80] G. Long, G. Adamo, J. Tian, M. Klein, H. N. S. Krishnamoorthy, E. Feltri, H. Wang, C. Soci, *Nat. Commun.* **2022**, *13*, 1551.
- [81] J. Mendoza-Carreño, P. Molet, C. Otero-Martínez, M. I. Alonso, L. Polavarapu, A. Mihi, *Adv. Mater.* **2023**, *35*, 2210477.
- [82] I. C. Seo, S. Kim, B. H. Woo, I.-S. Chung, Y. C. Jun, *Nanophotonics* **2020**, *9*, 4565.
- [83] Y. Zhang, M. Zhao, J. Wang, W. Liu, B. Wang, S. Hu, G. Lu, A. Chen, J. Cui, W. Zhang, C. W. Hsu, X. Liu, L. Shi, H. Yin, J. Zi, *Sci. Bull.* **2021**, *66*, 824.
- [84] B. Luk'Yanchuk, N. I. Zheludev, S. A. Maier, N. J. Halas, P. Nordlander, H. Giessen, C. T. Chong, *Nat. Mater.* **2010**, *9*, 707.
- [85] A. B. Khanikaev, C. Wu, G. Shvets, *Nanophotonics* **2013**, *2*, 247.
- [86] B. Zhen, S.-L. Chua, J. Lee, A. W. Rodriguez, X. Liang, S. G. Johnson, J. D. Joannopoulos, M. Soljačić, O. Shapira, *Proc. Natl. Acad. Sci. U.S.A.* **2013**, *110*, 13711.
- [87] M. F. Limonov, M. V. Rybin, A. N. Poddubny, Y. S. Kivshar, *Nat. Photonics* **2017**, *11*, 543.
- [88] S. Yuan, X. Qiu, C. Cui, L. Zhu, Y. Wang, Y. Li, J. Song, Q. Huang, J. Xia, *ACS Nano* **2017**, *11*, 10704.
- [89] S. Liu, A. Vaskin, S. Addamane, B. Leung, M.-C. Tsai, Y. Yang, P. P. Vabishchevich, G. A. Keeler, G. Wang, X. He, M. B. Sinclair, I. Staude, I. Brener, *Nano Lett.* **2018**, *18*, 6906.
- [90] F. Muckel, K. N. Guye, S. M. Gallagher, Y. Liu, D. S. Ginger, *Nano Lett.* **2021**, *21*, 6124.
- [91] C. Wu, N. Arju, G. Kelp, J. A. Fan, J. Dominguez, E. Gonzales, E. Tutuc, I. Brener, G. Shvets, *Nat. Commun.* **2014**, *5*, 3892.
- [92] B. Hopkins, A. N. Poddubny, A. E. Miroshnichenko, Y. S. Kivshar, *Laser Photonics Rev.* **2016**, *10*, 137.
- [93] A. V. Kondratov, M. V. Gorkunov, A. N. Darinskii, R. V. Gainutdinov, O. Y. Rogov, A. A. Ezhov, V. V. Artemov, *Phys. Rev. B* **2016**, *93*, 195418.
- [94] Y. Hwang, S. Lee, S. Kim, J. Lin, X.-C. Yuan, *ACS Photonics* **2018**, *5*, 4538.
- [95] X. Piao, S. Yu, N. Park, in *Fano Resonances In Optics And Microwaves* (Eds: E. Kamenetskii, A. Sadreev, A. Miroshnichenko), Springer, Cham Switzerland **2018**.
- [96] Z. Liu, Y. Xu, C. Y. Ji, S. Chen, X. Li, X. Zhang, Y. Yao, J. Li, *Adv. Mater.* **2020**, *32*, 1907077.
- [97] J. Tian, G. Adamo, H. Liu, M. Klein, S. Han, H. Liu, C. Soci, *Adv. Mater.* **2022**, *34*, 2109157.
- [98] Y. Chen, J. Feng, Y. Huang, W. Chen, R. Su, S. Ghosh, Y. Hou, Q. Xiong, C.-W. Qiu, *Nat. Mater.* **2023**, *22*, 1065.
- [99] I. Fernandez-Corbaton, M. Fruhnert, C. Rockstuhl, *Phys. Rev. X* **2016**, *6*, 031013.
- [100] C. W. Hsu, B. Zhen, A. Stone, J. D. Joannopoulos, M. Soljačić, *Nat. Rev. Mater.* **2016**, *1*, 16048.
- [101] K. Koshelev, G. Favraud, A. Bogdanov, Y. Kivshar, A. Fratallocchi, *Nanophotonics* **2019**, *8*, 725.
- [102] A. Kodigala, T. Lepetit, Q. Gu, B. Bahari, Y. Fainman, B. Kanté, *Nature* **2017**, *541*, 196.
- [103] S. T. Ha, Y. H. Fu, N. K. Emani, Z. Pan, R. M. Bakker, R. Paniagua-Domínguez, A. I. Kuznetsov, *Nat. Nanotechnol.* **2018**, *13*, 1042.
- [104] A. Tittl, A. Leitis, M. Liu, F. Yesilkoy, D.-Y. Choi, D. N. Neshev, Y. S. Kivshar, H. Altug, *Science* **2018**, *360*, 1105.
- [105] F. Yesilkoy, E. R. Arvelo, Y. Jahani, M. Liu, A. Tittl, V. Cevher, Y. Kivshar, H. Altug, *Nat. Photonics* **2019**, *13*, 390.
- [106] C. Huang, C. Zhang, S. Xiao, Y. Wang, Y. Fan, Y. Liu, N. Zhang, G. Qu, H. Ji, J. Han, L. Ge, Y. Kivshar, Q. Song, *Science* **2020**, *367*, 1018.
- [107] K. Koshelev, S. Kruk, E. Melik-Gaykazyan, J.-H. Choi, A. Bogdanov, H.-G. Park, Y. Kivshar, *Science* **2020**, *367*, 288.
- [108] M.-S. Hwang, H.-C. Lee, K.-H. Kim, K.-Y. Jeong, S.-H. Kwon, K. Koshelev, Y. Kivshar, H.-G. Park, *Nat. Commun.* **2021**, *12*, 4135.
- [109] M. V. Gorkunov, A. A. Antonov, Y. S. Kivshar, *Phys. Rev. Lett.* **2020**, *125*, 093903.
- [110] M. V. Gorkunov, A. A. Antonov, V. R. Tuz, A. S. Kupriianov, Y. S. Kivshar, *Adv. Opt. Mater.* **2021**, *9*, 2100797.
- [111] A. Overvig, N. Yu, A. Alù, *Phys. Rev. Lett.* **2021**, *126*, 073001.
- [112] A. C. Overvig, S. A. Mann, A. Alù, *Phys. Rev. X* **2021**, *11*, 021050.
- [113] X. Zhang, Y. Liu, J. Han, Y. Kivshar, Q. Song, *Science* **2022**, *377*, 1215.
- [114] J. Wu, X. Xu, X. Su, S. Zhao, C. Wu, Y. Sun, Y. Li, F. Wu, Z. Guo, H. Jiang, H. Chen, *Phys. Rev. Appl.* **2021**, *16*, 064018.
- [115] Y. Chen, H. Deng, X. Sha, W. Chen, R. Wang, Y.-H. Chen, D. Wu, J. Chu, Y. S. Kivshar, S. Xiao, C.-W. Qiu, *Nature* **2023**, *613*, 474.
- [116] L. Kühner, F. J. Wendisch, A. A. Antonov, J. Bürger, L. Hüttenhofer, L. de S. Menezes, S. A. Maier, M. V. Gorkunov, Y. Kivshar, A. Tittl, *Light Sci. Appl.* **2023**, *12*, 250.
- [117] L. D. Landau, E. M. Lifshitz, L. P. Pitaevskii, in *Electrodynamics Of Continuous Media*, Butterworth-Heinemann, Oxford, England **1984**.
- [118] L. Novotny, B. Hecht, in *Principles Of Nano-Optics*, Cambridge University Press, Cambridge, England **2012**.

- [119] A. Vaskin, R. Kolkowski, A. F. Koenderink, I. Staude, *Nanophotonics* **2019**, *8*, 1151.
- [120] G. Lozano, D. J. Louwers, S. R. Rodríguez, S. Murai, O. T. Jansen, M. A. Verschuuren, J. Gómez Rivas, *Light Sci. Appl.* **2013**, *2*, e66.
- [121] S. R. K. Rodriguez, Y. T. Chen, T. P. Steinbusch, M. A. Verschuuren, A. F. Koenderink, J. G. Rivas, *Phys. Rev. B* **2014**, *90*, 235406.
- [122] M. Ramezani, G. Lozano, M. A. Verschuuren, J. Gómez-Rivas, *Phys. Rev. B* **2016**, *94*, 125406.
- [123] S. Zhang, E. R. Martins, A. G. Diyaf, J. I. Wilson, G. A. Turnbull, I. D. Samuel, *Synth. Met.* **2015**, *205*, 127.
- [124] J. W. Yoon, S. H. Song, R. Magnusson, *Sci. Rep.* **2015**, *5*, 18301.
- [125] T. J. Seok, A. Jamshidi, M. Kim, S. Dhuey, A. Lakhani, H. Choo, P. J. Schuck, S. Cabrini, A. M. Schwartzberg, J. Bokor, E. Yablonovitch, M. C. Wu, *Nano Lett.* **2011**, *11*, 2606.
- [126] H. He, M. Cen, J. Wang, Y. Xu, J. Liu, W. Cai, D. Kong, K. Li, D. Luo, T. Cao, Y. J. Liu, *ACS Appl. Mater. Interfaces* **2022**, *14*, 53981.
- [127] Y.-T. Lee, M.-H. Chen, Y.-L. Ho, Z. Wang, Y.-C. Lee, J.-J. Delaunay, *ACS Appl. Mater. Interfaces* **2023**, *15*, 36945.
- [128] K. Konishi, M. Nomura, N. Kumagai, S. Iwamoto, Y. Arakawa, M. Kuwata-Gonokami, *Phys. Rev. Lett.* **2011**, *106*, 057402.
- [129] A. A. Maksimov, I. I. Tartakovskii, E. V. Filatov, S. V. Lobanov, N. A. Gippius, S. G. Tikhodeev, C. S. Schneider, M. Kamp, S. Maier, S. Höfling, V. D. Kulakovskii, *Phys. Rev. B* **2014**, *89*, 045316.
- [130] S. V. Lobanov, S. G. Tikhodeev, N. A. Gippius, A. A. Maksimov, E. V. Filatov, I. I. Tartakovskii, V. D. Kulakovskii, T. Weiss, C. Schneider, J. Geßler, M. Kamp, S. Höfling, *Phys. Rev. B* **2015**, *92*, 205309.
- [131] N. Meinzer, E. Hendry, W. L. Barnes, *Phys. Rev. B* **2013**, *88*, 041407.
- [132] M. Cotrufo, C. I. Osorio, A. F. Koenderink, *ACS Nano* **2016**, *10*, 3389.
- [133] Y. Sun, Z. Hu, K. Shi, T. Guo, Y. Xing, Y. Jin, S. He, *Adv. Opt. Mater.* **2023**, *11*, 2300197.
- [134] S. S. Kruk, M. Decker, I. Staude, S. Schlecht, M. Greppmair, D. N. Neshev, Y. S. Kivshar, *ACS Photonics* **2014**, *1*, 1218.
- [135] Z. Wang, Y. Wang, G. Adamo, J. Teng, H. Sun, *Laser Photonics Rev.* **2019**, *13*, 1800276.
- [136] K. Rong, B. Wang, A. Reuven, E. Maguid, B. Cohn, V. Kleiner, S. Katznelson, E. Koren, E. Hasman, *Nat. Nanotechnol.* **2020**, *15*, 927.
- [137] K. Rong, X. Duan, B. Wang, D. Reichenberg, A. Cohen, C.-I. Liu, P. K. Mohapatra, A. Patsha, V. Gorovoy, S. Mukherjee, V. Kleiner, A. Ismach, E. Koren, E. Hasman, *Nat. Mater.* **2023**, *22*, 1085.
- [138] S.-H. Gong, F. Alpeggiani, B. Sciacca, E. C. Garnett, L. Kuipers, *Science* **2018**, *359*, 443.
- [139] J. Wang, H. Li, Y. Ma, M. Zhao, W. Liu, B. Wang, S. Wu, X. Liu, L. Shi, T. Jiang, J. Zi, *Light Sci. Appl.* **2020**, *9*, 148.
- [140] Y. Liu, S. C. Lau, W.-H. Cheng, A. Johnson, Q. Li, E. Simmerman, O. Karni, J. Hu, F. Liu, M. L. Brongersma, T. F. Heinz, J. A. Dionne, *Nano Lett.* **2023**, *23*, 6124.
- [141] P. Chen, T. W. Lo, Y. Fan, S. Wang, H. Huang, D. Lei, *Adv. Opt. Mater.* **2020**, *8*, 1901233.
- [142] S. Fan, J. D. Joannopoulos, *Phys. Rev. B* **2002**, *65*, 235112.
- [143] S. G. Tikhodeev, A. L. Yablonskii, E. A. Muljarov, N. A. Gippius, T. Ishihara, *Phys. Rev. B* **2002**, *66*, 045102.
- [144] Y. H. Ko, R. Magnusson, *Optica* **2018**, *5*, 289.
- [145] Y. Ohno, D. K. Young, B. Beschoten, F. Matsukura, H. Ohno, D. D. Awschalom, *Nature* **1999**, *402*, 790.
- [146] R. Fiederling, M. Keim, G. Reuscher, W. Ossau, G. Schmidt, A. Waag, L. W. Moltenkamp, *Nature* **1999**, *402*, 787.
- [147] J. Wang, C. Zhang, H. Liu, R. McLaughlin, Y. Zhai, S. R. Vardeny, X. Liu, S. McGill, D. Semenov, H. Guo, R. Tsuchikawa, V. V. Deshpande, D. Sun, Z. V. Vardeny, *Nat. Commun.* **2019**, *10*, 129.
- [148] Y.-H. Kim, Y. Zhai, H. Lu, X. Pan, C. Xiao, E. A. Gaubling, S. P. Harvey, J. J. Berry, Z. V. Vardeny, J. M. Luther, M. C. Beard, *Science* **2021**, *371*, 1129.
- [149] A. Maksimov, E. V. Filatov, I. I. Tartakovskii, V. D. Kulakovskii, S. Tikhodeev, C. Schneider, S. Höfling, *Phys. Rev. Appl.* **2022**, *17*, L021001.
- [150] J. Jia, X. Cao, X. Ma, J. De, J. Yao, S. Schumacher, Q. Liao, H. Fu, *Nat. Commun.* **2023**, *14*, 31.
- [151] Y. J. Zhang, T. Oka, R. Suzuki, J. T. Ye, Y. Iwasa, *Science* **2014**, *344*, 725.
- [152] J. Pu, W. Zhang, H. Matsuoka, Y. Kobayashi, Y. Takaguchi, Y. Miyata, K. Matsuda, Y. Miyauchi, T. Takenobu, *Adv. Mater.* **2021**, *33*, 2100601.
- [153] J.-J. Greffet, R. Carminati, K. Joulain, J.-P. Mulet, S. Mainguy, Y. Chen, *Nature* **2002**, *416*, 61.
- [154] L. Shi, T. K. Hakala, H. T. Rekola, J.-P. Martikainen, R. J. Moerland, P. Törmä, *Phys. Rev. Lett.* **2014**, *112*, 153002.
- [155] L. Shi, X. Yuan, Y. Zhang, T. Hakala, S. Yin, D. Han, X. Zhu, B. Zhang, X. Liu, P. Törmä, W. Lu, J. Zi, *Laser Photonics Rev.* **2014**, *8*, 717.
- [156] K. Voronin, A. S. Taradin, M. V. Gorkunov, D. G. Baranov, *Acc Photonics* **2022**, *9*, 2652.
- [157] M. V. Gorkunov, A. A. Antonov, Y. S. Kivshar, presented at *2023 Days on Diffraction (DD)*, St. Petersburg, Russian Federation, June **2023**.
- [158] D. Sanvitto, S. Kéna-Cohen, *Nat. Mater.* **2016**, *15*, 1061.
- [159] S. Ghosh, R. Su, J. Zhao, A. Fieramosca, J. Wu, T. Li, Q. Zhang, F. Li, Z. Chen, T. Liew, D. Sanvitto, Q. Xiong, *Photonics Insights* **2022**, *1*, R04.
- [160] T. Fujita, Y. Sato, T. Kuitani, T. Ishihara, *Phys. Rev. B* **1998**, *57*, 12428.
- [161] G. Lanty, A. Brehier, R. Parashkov, J.S. Lauret, E. Deleporte, *New J. Phys.* **2008**, *10*, 065007.
- [162] J. Wang, R. Su, J. Xing, D. Bao, C. Diederichs, S. Liu, T. C. Liew, Z. Chen, Q. Xiong, *ACS Nano* **2018**, *12*, 8382.
- [163] N. H. M. Dang, D. Gerace, E. Drouard, G. Trippé-Allard, F. Lédée, R. Mazurczyk, E. Deleporte, C. Seassal, H. S. Nguyen, *Nano Lett.* **2020**, *20*, 2113.
- [164] I. A. Al-Ani, K. As' Ham, L. Huang, A. E. Miroshnichenko, W. Lei, H. T. Hattori, *Adv. Opt. Mater.* **2022**, *10*, 2101120.
- [165] W. Liu, Z. Ji, Y. Wang, G. Modi, M. Hwang, B. Zheng, V. J. Sorger, A. Pan, R. Agarwal, *Science* **2020**, *370*, 600.
- [166] N. H. M. Dang, S. Zanotti, E. Drouard, C. Chevalier, G. Trippé-Allard, M. Amara, E. Deleporte, V. Ardizzone, D. Sanvitto, L. C. Andreani, C. Seassal, D. Gerace, H. S. Nguyen, *Adv. Opt. Mater.* **2022**, *10*, 2102386.
- [167] B. Zhen, C. W. Hsu, L. Lu, A. D. Stone, M. Soljačić, *Phys. Rev. Lett.* **2014**, *113*, 257401.
- [168] T. Yoda, M. Notomi, *Phys. Rev. Lett.* **2020**, *125*, 053902.
- [169] X. Yin, C. Peng, *Photonics Res.* **2020**, *8*, B25.
- [170] W. Liu, W. Liu, L. Shi, Y. Kivshar, *Nanophotonics* **2021**, *10*, 1469.
- [171] D. G. Baranov, C. Schäfer, M. V. Gorkunov, *ACS Photonics* **2023**, *10*, 2440.
- [172] R. R. Riso, L. Grazioli, E. Ronca, T. Giovannini, H. Koch, *Phys. Rev. X* **2023**, *13*, 031002.
- [173] A. Amo, T. C. H. Liew, C. Adrados, R. Houdré, E. Giacobino, A. V. Kavokin, A. V. Bramati, *Nat. Photonics* **2010**, *4*, 361.
- [174] D. Ballarini, M. De Giorgi, E. Cancellieri, R. Houdré, E. Giacobino, R. Cingolani, A. Bramati, G. Gigli, D. Sanvitto, *Nat. Commun.* **2013**, *4*, 1778.
- [175] A. V. Zasedatelev, A. V. Baranikov, D. Urbonas, F. Scafrimuto, U. Scherf, T. Stöferle, R. F. Mahrt, P. G. Lagoudakis, *Nat. Photonics* **2019**, *13*, 378.
- [176] A. V. Kavokin, J. J. Baumberg, G. Malpuech, F. P. Laussy, *Microcavities*, Oxford Univ. Press, Oxford, England **2017**.
- [177] C. Anton-Solanas, M. Waldherr, M. Klaas, H. Suchomel, T. H. Harder, H. Cai, E. Sedov, S. Klemmt, A. V. Kavokin,

- S. Tongay, K. Watanabe, T. Taniguchi, S. Höfling, C. Schneider, *Nat. Mater.* **2021**, 20, 1233.
- [178] V. Ardizzone, F. Riminucci, S. Zanotti, A. Gianfrate, M. Efthymiou-Tsironi, D. G. Suárez-Forero, F. Todisco, M. De Giorgi, D. Trypogeorgos, G. Gigli, K. Baldwin, L. Pfeiffer, D. Ballarini, H. S. Nguyen, D. Gerace, D. Sanvitto, *Nature* **2022**, 605, 447.
- [179] N. Y. Kim, Y. Yamamoto, in *Quantum Simulations With Photons And Polaritons: Merging Quantum Optics With Condensed Matter Physics* (Eds: D. G. Angelakis), Springer International Publishing, Cham Switzerland **2017**.
- [180] M. Vladimirova, S. Cronenberger, D. Scalbert, K. V. Kavokin, A. Miard, A. Lemaître, J. Bloch, D. Solnyshkov, G. Malpuech, A. V. Kavokin, *Phys. Rev. B* **2010**, 82, 075301.
- [181] A. Fieramosca, L. Polimeno, V. Ardizzone, L. De Marco, M. Pugliese, V. Maiorano, M. De Giorgi, L. Dominici, G. Gigli, D. Gerace, D. Ballarini, D. Sanvitto, *Sci. Adv.* **2019**, 5, eaav9967.



Jungho Han received his B.S. degree from Ulsan National Institute of Science and Technology (UNIST) in 2023 and is currently a Ph.D. student in materials science and engineering at the same institute, under the supervision of Prof. Young Chul Jun. His current research interests include chiral emission, which exhibits a high degree of circular polarization, with potential applications ranging from displays and optical storage to medical diagnostics.



Heejoo Jang received her B.S. degree from Kongju National University in 2023 and is currently a M.S. student in Graduate School of Semiconductor Materials and Devices Engineering at UNIST. Her current research interests include chiral metasurface and bound states in the continuum.



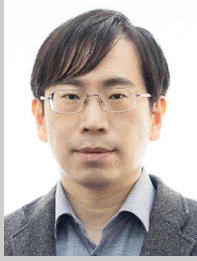
Yeonsoo Lim received his B.S. degree from Korea university of technology and education in 2018. He is currently a Ph.D. student in materials science and engineering at UNIST. His current research interests include metasurfaces about chiral emission, bound states in the continuum, topology, and their experimental investigation.



Seongheon Kim received his B.S. degree in material science and engineering from UNIST in 2019. He is currently pursuing a Ph.D. in the Department of Material Science and Engineering at UNIST. His research interests include chiral emissive metasurfaces and chiral bound states in the continuum, and their potential applications in displays, optical quantum communication, and biosensing.



Jeheon Lee graduated with a bachelor's degree in the School of Physics from UNIST in 2024. He is currently a graduate student in the combined Master's-Doctoral program in materials science and engineering at UNIST. He is interested in topological photonics, chiral emission, dielectric metasurfaces, etc., particularly focusing on chiral perfect absorbers via computational inverse design.



Young Chul Jun has received his Ph.D. at Stanford University (Applied Physics) in 2011. He is currently an associate professor at UNIST (Materials science and engineering). He has been working on various topics in nanophotonics and metamaterials research, including surface plasmon resonances, epsilon-near-zero (ENZ) materials, perfect absorbers, Fano resonances, spoof surface plasmons, and 3D/4D printing. More recently, his group has conducted intense research on chiral emission and exciton polaritons in perovskite metasurfaces, bound states in the continuum, exceptional points, topological singularities and phase transitions, etc.